JOURNAL OF GEOPHYSICAL RESEARCH, VOL. 115, E07009, doi:10.1029/2009JE003433, 2010

Impact cratering on the H chondrite parent asteroid

Axel Wittmann,[1] Timothy D. Swindle,[2] Leah C. Cheek,[3] Elizabeth A. Frank,[4] and David A. Kring[1]

Received 18 May 2009; revised 26 January 2010; accepted 12 February 2010; published 20 July 2010.

[1] This paper reports petrological data for LaPaz Icefield 02240, 03922, 031125, 031173, 031308, 04462, and 04751, which are meteoritic samples of clast-rich impact melt rocks from the H chondrite parent asteroid. The size distribution and metallographic characteristics of Fe-Ni metal in the melts indicate very rapid 1 to 40°C/s cooling in the temperature range between >1500 and ~950°C when the clast-melt mixtures were thermally equilibrating. Cooling slowed to values between 10^{-3} and 10^{-2}°C/s in the temperature range between 700 and 400°C when the melt rocks were cooling to their surroundings. These data suggest that the rocks cooled near the surface of the H chondrite asteroid within suevitic impact deposits. Integrating these data with the petrologic characteristics of other H chondrite melt rocks and their radioisotopic ages indicates that the H chondrite asteroid suffered at least one large impact event while still cooling from endogenous metamorphism at ~4500 Ma; this impact must have degraded the asteroid's integrity but did not cause shattering. Impact events in the era between ~4100 and ~3600 Ma produced melt volumes large enough to allow segregation of metal and troilite from silicate melts, possibly within continuous impact melt sheets contained in craters. The impact record after 3600 Ma does not display such assemblages, which suggests a decrease in the rate of large impact events or a catastrophic size reduction of the H chondrite parent asteroid at around this time.

Citation: Wittmann, A., T. D. Swindle, L. C. Cheek, E. A. Frank, and D. A. Kring (2010), Impact cratering on the H chondrite parent asteroid, *J. Geophys. Res.*, *115*, E07009, doi:10.1029/2009JE003433.

1. Introduction

[2] The fall statistics of meteorites are dominated by ordinary chondrites: L chondrites are recorded in 38%, H chondrites in 34.1% and LL chondrites in 7.9% of all cases [*Burbine et al.*, 2002]. Ordinary chondrites are characterized by oxygen isotope compositions that plot above the terrestrial fractionation line, a large volume percentage of chondrules, and only 10–15 vol % fine-grained matrix. The high-iron (H) chemical group of ordinary chondrites is distinguished by high siderophile element content, relatively small chondrules (~0.3 mm), and oxygen isotope compositions that are closer to the terrestrial fractionation line than those of other ordinary chondrites [*Brearley and Jones*, 1998]. Among officially classified meteorites, the 14,990 H chondrites comprise by far the most recorded specimens according to the Meteoritical Bulletin Database (of 37,769 meteorite specimen with official names according to http://tin.er.usgs.gov/meteor/metbull.php, accessed 13 May 2009). Thus, H chondrites provide one of the most complete pictures of an asteroid in the Solar System. These chondrites are often used to study nebular processes, but most of them have been altered by thermal metamorphic and shock metamorphic processes that occurred after planetesimal accretion. While endogenous activity ceased long ago, impact cratering has affected the evolution of the H chondrite asteroid over its entire 4.5 Ga lifetime. To better understand that collisional evolution, this study examines H chondrite whole rock impact melts that were produced in hypervelocity impacts, evaluates the conditions of their emplacement and integrates that information with previous studies of shocked H chondrites [e.g., *Taylor and Heymann*, 1971; *Smith and Goldstein*, 1977; *Scott*, 1982; *Stöffler et al.*, 1991; *Bogard*, 1995].

1.1. H Chondrite Parent Asteroid, Its Thermal Structure, and Evidence for Impacts

[3] Petrophysical properties, thermal metamorphic cooling rates, and isotopic closure ages of H chondrites have been used to generate a model for the parent asteroid that is characterized by an onion skin structure with progressively lower metamorphic zones from the center outward [*Bennett and McSween*, 1996; *Akridge et al.*, 1998; *McSween et al.*, 2002; *Trieloff et al.*, 2003]. A diameter of ~90 to 200 km is implied by these models for the H chondrite parent

[1]Lunar and Planetary Institute, Houston, Texas, USA.
[2]Lunar and Planetary Laboratory, University of Arizona, Tucson, Arizona, USA.
[3]Department of Geological Sciences, Brown University, Providence, Rhode Island, USA.
[4]Department of Earth and Environmental Sciences, Rensselaer Polytechnic Institute, Troy, New York, USA.

0148-0227/10/2009JE003433

asteroid. Metamorphism is thought to be dominated by radiogenic heating, primarily due to the decay of ^{26}Al in the first ~10 Ma, with metamorphic cooling constrained to within the first 60 Ma after formation of Ca-Al-rich inclusions (CAI) [*Göpel et al.*, 1994]. Recent thermochronometric modeling of the H chondrite asteroid by *Kleine et al.* [2008] suggests delay of accretion by 1.5–2 Ma and a metamorphic peak at ~10 Ma after formation of CAI. Delayed accretion of the H chondrite parent asteroid is consistent with the finite difference models of *Hevey and Sanders* [2006] and the numerical models of *Sahijpal et al.* [2007] that explore its thermal evolution. These authors conclude that parent asteroids with radii as small as 20 km would undergo endogenous differentiation if they accreted immediately after the formation of CAI. Because the H chondrite parent asteroid did not undergo significant differentiation, delayed accretion is required.

[4] An analysis by *Lipschutz and Schultz* [2007] shows that about 86% of H chondrites exhibit a diagnostic shock metamorphic overprint. These include shock-melted material that was mixed with surviving relict target rocks to produce clast-rich impact melts [*Stöffler and Grieve*, 2007]. Such melts may remain in the crater where they are incorporated into pools within crater fill or, alternatively, get ejected to the surface of the asteroid. In other cases, melt may be injected in veins into the asteroid beneath the crater floor [*Stöffler et al.*, 1991; *Keil et al.*, 1997; *Stöffler and Grieve*, 2007]. Typically, there are two phases to the solidification of these mixed materials. Initially, the superheated impact melt and relatively cold relict material thermally equilibrates (stage 1 cooling). Then, the mixture cools radiatively or conductively to the surroundings (stage 2 cooling) [*Onorato et al.*, 1978]. These cooling rates can be used to deduce the size of the melt volumes, their relative burial depth, and, thus, place limits on the size of the cratering event.

[5] The potential to reconstruct these impact events continues to grow as additional impact melt samples are located. *Keil et al.* [1997] estimated that only <0.001 vol % of impact-generated debris would be melted over the typical lifetime of an asteroid, yet the proportion of melt being found in meteorite collections is 2–3 orders of magnitude higher (Table A1).

[6] The timing of the impact events is critical to the evolution of the H chondrite parent asteroid. *Bogard* [1995], *Grier et al.* [2004], and more recently *Swindle et al.* [2009] presented summaries of radioisotopic ages derived from impact melted and severely shocked H chondrites. Impact melts with ancient (>4.4 Ga) ages indicate the simple "onion skin" model of endogeneous thermal metamorphism was repeatedly disturbed. Those disturbances may be responsible for discrepancies of petrologic types with metallographic cooling rates in certain H chondrites, which were interpreted by *Taylor et al.* [1987] as records of intense cratering on the H chondrite parent asteroid during cooling from peak metamorphic temperatures. However, modeling by *Akridge et al.* [1998] suggests that thermal insulation by regolith can produce the full range of known metallographic cooling rates in a megaregolith. These authors also infer that types 3–6 H chondrites would occur within 10 km of the asteroid's surface. In contrast, *Grimm* [1985] evokes catastrophic impact disruption during metamorphism and rapid gravitational reassembly in order to explain discrepancies between cooling rates and petrologic type in certain H chondrites. *Benoit and Sears* [1992], *Rubin and Bottke* [2009], and *Swindle et al.* [2009] discuss the possibility that the H chondrites that currently reach Earth stem from an asteroid family, which resulted from the catastrophic disruption of the H chondrite asteroid. These discussions mainly pertain to Ar-Ar ages and subrecent collisional events involving material of H chondrite parentage, which is recorded by cosmic ray exposure ages (CRE). Based on their CRE analyses, *Graf and Marti* [1995] identified a major collisional event at 7 to 8 Ma ago that produced ~45% of H chondrites that currently reach Earth, mostly petrologic types 4 and 5; an earlier event at ~60 Ma produced type 4–6 H chondrites, and at 33 Ma, debris was sourced from all petrological types. Another collision at 24 Ma predominantly launched H6 chondrites [*Graf and Marti*, 1995]. More evidence for collisions involving H chondrite parent material can be gleaned from impact craters on Earth. To date, traces of one ~1 km diameter H chondrite impactor have been identified in the impact melt rocks of the ~73 Ma old, ~22 km diameter Lappajärvi impact crater [*Tagle et al.*, 2007].

1.2. Intent of Study

[7] Seven H chondrite impact melt samples are examined in order to constrain physical parameters for their formation and emplacement. Petrologic analyses are used to assess the type of material entrained in the melts and potentially the depth of excavation. Metallographic cooling rates are used to determine the volume of melt that was produced, its depth of burial, and the type of impact deposit. This information is integrated with published radioisotopic ages for some of these samples and other H chondrite impact melts to reconstruct the collisional history of their parent asteroid.

2. Samples and Methods

[8] Samples studied are H chondrite impact melts from Antarctica's LaPaz Icefield (LAP 02240, 03922, 031125, 031173, 031308, 04462, and 04751) with masses between 1.4 and 45.9 g [*Russell et al.*, 2005; *Connolly et al.*, 2007a, 2007b; *Weisberg et al.*, 2008] (Table 1). Petrographic descriptions are based on macroscopic inspection of sample specimens (Figures 1a–1f), optical microscopic investigations and scanning electron microscopy. Modal compositions were determined for the bulk samples from scanned images of 2.54 cm diameter petrographic thin sections (Figures 2a–2b). This yielded the relative proportions of clasts >~1 mm versus impact melt. Point counting under reflected light of a minimum of 1087 points per thin section was conducted at ×500 magnification and a step size of 100 μm. The discriminated components are (1) lithic clasts <~1 mm in size that were entrained in the melt, (2) the silicate melt matrix, (3) particles of Fe-Ni metal and troilite, whose relative sizes were recorded in arbitrary bins, and (4) voids and unidentified alteration features. Because sulfide and metal could not be discriminated in submicron particles, modal proportions of metal and troilite in that size bin are reported as combined metal and troilite.

[9] Geochemical data was obtained from electron microprobe analysis at the NASA Johnson Space Center, Houston,

Table 1. Samples, Their Modal Composition, and Petrologic Type[a]

Sample Thin Section	Thin Section Scale[b]			Microscopic Scale[c]		Modal Composition of Impact Melt			
	Lithic Clasts		Melt (%)	Lithic Clasts (%)	Silicate Melt (%)	Oxides (%)	Metal and Troilite (%)	Points Counted	Petrologic Type[e]
	Millimeter[d]	Percent							
LAP 02240, 8	3.3	23.4	76.6	17.2	68.8	86	14	1720	5
LAP 03922, 6	6.5	47.5	52.5	15.25	84.75	84.75	15.25	1416	4–5
LAP 04751, 6	4	39.2	60.8	13.2	69.4	82.6	17.4	1762	4–5
LAP 031125, 4	ND	NA	100	10.6	82.1	92.7	7.3	1504	6
LAP 031173, 6	5	23.4	76.6	8.8	75.4	84.3	15.7	1992	5
LAP 031308, 4	9.6	57.8	42.2	11.8	72.9	84.7	15.3	1087	5
LAP 04462, 8	ND	NA	100	6.1	78.4	84.5	15.5	2052	5

[a]NA, not applicable; ND, none detected.
[b]Clasts larger than ~1 mm, areal proportions determined by image analysis.
[c]Modal composition of impact melt portion in thin section determined by point counting under reflected light, magnification 500×, step spacing 100 μm; data normalized, excluding voids and alteration features.
[d]Minimum size of largest lithic clast in thin section.
[e]Reflecting thermal metamorphism determined from petrologic characteristics of lithic clasts after *Van Schmus and Wood* [1967].

using a Cameca SX-100 with five wavelength dispersive spectrometers. Peak positions and intensities of individual elements were calibrated and monitored with well-characterized standards from the NASA Johnson Space Center standard collection. Silicate minerals were analyzed using an accelerating voltage of 15 keV, a beam current of 15 nA and a beam diameter of 1 μm. To reduce volatilization, counting times for the measurements were 10 s for Na and K, but 20 s for Si, Fe, Mg, Ca, Cr, Al, Ti, Mn, Ni, and P. For analyses of Fe-Ni metal and sulfide, an accelerating voltage of 15 keV and a beam current of 20 nA was used to determine the abundances of Fe, Ni, Co, Cr, Mn, Cu, Zn, Ti, Si, V, P, Ca, Mg, and S.

[10] Metallographic cooling rates were determined for stage 1 cooling. This describes cooling of the superheated impact melt to ~950°C, the approximate solidus of troilite associated with meteoritic alloys [*Scott*, 1982]. As per the method of *Scott* [1982], the spacing of metal cells in the largest, continuous metal troilite particles was measured in the seven LAP samples. The same method was applied to a thick section of the H chondrite impact melt Orvinio because a previous study [*Grier et al.*, 2004] had not evaluated its stage 1 cooling rate.

[11] Preliminary descriptions and cooling rate calculations for two of the seven LAP meteorites (LAP 02240 and 04751) have appeared in abstract form [*Cheek and Kring*, 2008; *Frank et al.*, 2009].

3. Results

3.1. Petrography

[12] After sample processing, the seven meteorites consist of up to 4 cm size fragments of dark olive gray–colored rocks (Figures 1a–1f). Up to cm size lithic clasts entrained in impact melt are visible in some of these samples (e.g., Figures 1a, 1b, and 1e). Occasionally, bubbly to angular-shaped, up to ~mm size voids occur in the homogenous melt domains that are not associated with alteration and are, therefore, likely degassing vesicles (Figure 1c). Thin section petrography confirms that according to the IUGS classification for impactites [*Stöffler and Grieve*, 2007], all seven samples are clast-rich impact melt rocks (according to *Stöffler and Grieve* [2007], the term "impact melt rock" ought to replace the term "impact melt breccia"). In five of the seven thin sections examined, clastic material >1 mm represents 23 to 58% of the samples (Table 1). In these cases, the surviving lithic debris in the melt rocks is dominated by these macroscopic lithologic clasts. The melt in all samples also entrains microscopic lithic fragments and isolated crystal fragments, which represent all of the relict debris in two of the samples (LAP 031125 and 04462). In another sample (LAP 02240), the amount of this microscopic debris in the melt (17.2%) is nearly as large as the amount of macroscopic debris in the whole thin section (23.4%). The impact melt indicates shock pressures >75–90 GPa and a minimum increase in post shock temperature of 1500°C [*Stöffler et al.*, 1991].

[13] The samples are variably preserved. LAP 031125 was classified as weathering grade B and LAP 04751 as weathering grade B/C [*Connolly et al.*, 2007a]; all remaining samples were classified as weathering grade C [*Russell et al.*, 2005; *Connolly et al.*, 2007a, 2007b; *Weisberg et al.*, 2008]. Pronounced alteration features are only present in the thin sections of LAP 031173, LAP 31308, and LAP 03922, which are expressed as pervasive, wavy, subparallel fractures that are filled with Fe-oxides. These fractures did not rotate fragments and thus do not constitute brecciation. Although the oxidation consumed some of the metal, analyses of metal-sulfide assemblages was possible in all samples. In addition, this alteration does not appear to have significantly affected silicate compositions.

3.2. Modal Compositions

[14] Point counting under reflected light determined the proportions of oxide phases and Fe-Ni metal plus troilite (Table 1). Fe-Ni metal and troilite contents in the seven samples range between 7.3 and 17.4 vol %, with a typical value of ~15 vol %. *Mason* [1965] and *McSween et al.* [1991] found average normative contents of 23.9 wt % and 23.5 wt % Fe-Ni metal plus troilite in H chondrites, respectively. Recalculating these values to vol % with the specific gravities of 3.3 for silicates, 4.67 for troilite, 7.95 for Fe-Ni metal, and 4.7 for chromite as described by *Rubin and Jones* [2003], these values translate to an average normative 14.1 and 13 vol % Fe-Ni metal plus troilite in H chondrites, respectively. Thus, six of the seven samples

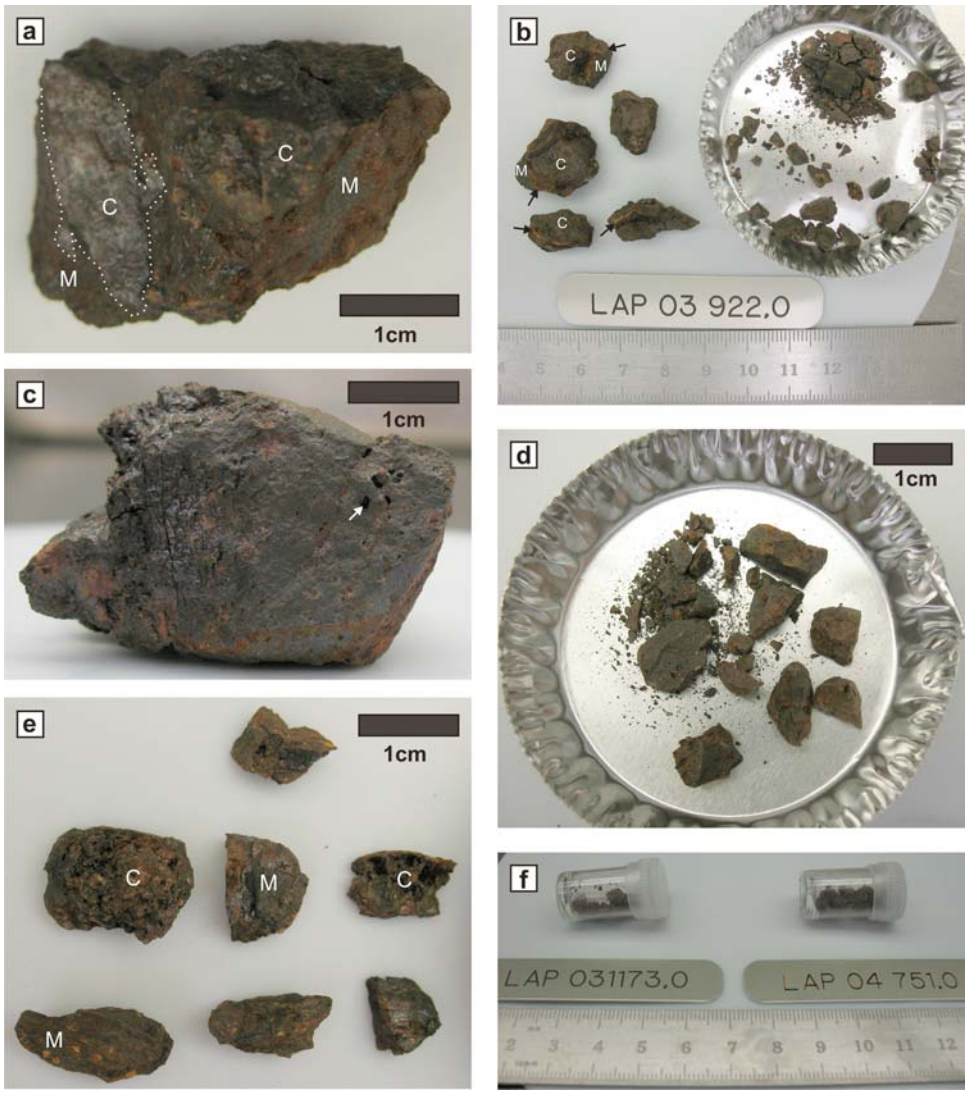

Figure 1. Specimen photographs of La Paz Ice field (LAP) meteorites. (a) Largest remaining piece of LAP 02240; note dotted line outlining boundary of a lithic clast (C) in melt matrix (M). (b) Remaining sample of LAP 03922; an orange contact (black arrows) formed at the contact of larger lithic clasts (C) toward surrounding melt (M). (c) Largest remaining piece of LAP 04462; note mm size voids that are not associated with alteration features and thus likely represent primary degassing vesicles. (d) Remaining sample material of LAP 031125. (e) Largest remaining pieces of LAP 031308; note uneven, angular surfaces that likely belong to lithic clasts (C) in contrast to smooth surfaces of melt with small entrained clasts (M). (f) Remaining sample material of LAP 031173 and LAP 04751.

have abundances of Fe-Ni metal and troilite that are consistent with H chondrites. The exception is LAP 031125, which is depleted in a metal-sulfide component. This depletion is not a product of weathering (this being the best preserved of all the specimens), but rather the result of metal-sulfide segregation during impact melting.

[15] Shock metamorphism is a well-known mechanism for redistributing metal and sulfide in chondrites [e.g., *Taylor et al.* 1979; *Britt and Pieters*, 1994; *Kring et al.*, 1996; *Grier et al.*, 2004]. Even in those specimens that have a full complement of their metal-sulfide components, the distribution of the metal and sulfide was modified. Two types of processes are discernable: (1) shock dissemination of metal and sulfide into micron to submicron particles in both the melt and relict clasts and (2) the agglomeration of metal in melts that remained fluid for sufficiently long times. Both processes are evident in the LAP samples.

[16] The size distribution of Fe-Ni metal and troilite particles in the seven melt rocks is illustrated in Figure 3a. Their size distributions exhibit a characteristic skew of higher proportions of larger metal-sulfide particle sizes in the samples that do not contain large clasts (Figure 3a). For example, the thin sections of LAP 031125 and LAP 04462 do not contain lithic clasts >1 mm and have the largest fractions of large metal-sulfide particles among the seven samples studied (Figure 3a). This suggests a relationship between the size of the metal-sulfide particles and the thermal histories of the melts. To explore this relationship,

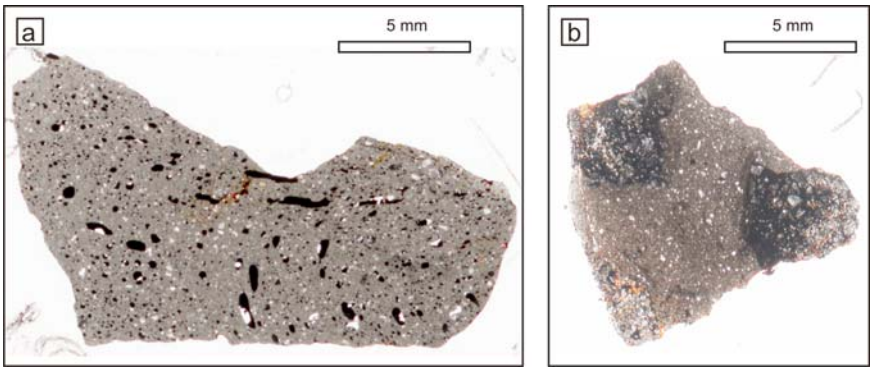

Figure 2. Thin section scans. (a) Sample LAP 04462, diameter of round thin section is 2.54 cm; note dark blebs of troilite and Fe-Ni metal in dark gray melt, which includes medium gray lithic clasts. Bright spots are voids. (b) Sample LAP 04751; note two shock blackened lithic breccia clasts in the northwest and east corners and a brecciated chondrite clast in the SSW corner of the sample. Clasts are floating in melt that contains abundant lithic clasts.

LAP 031173 was studied in greater detail (Figures 3b–3c). The thin section of this sample contains a lithic clast several mm in size that is surrounded by a quench zone of fine-grained melt. This quenched melt is adjacent to a melt that contains intermediate-size metal-sulfide particles, beyond which is another melt zone with even larger metal-sulfide particles. In Figure 3b, the size distributions of the metal troilite particles in these melt zones are shown. The clast-affected size distributions is also seen in LAP 03922, LAP 031308, and LAP 04751 (Figure 3b), which also contain quenched melt zones around mm size lithic clasts.

3.3. Petrologic Types of Relict Chondritic Material

[17] The thermal metamorphic grade of surviving lithic fragments was investigated according to the classification scheme of *Van Schmus and Wood* [1967] to identify the range of petrologic types of target materials involved in the respective impact events. Clast olivine compositions (Table A2) exhibit deviations from the means of FeO concentrations between ~1 and ~5%. This may suggest that these lithic clasts were mostly derived from equilibrated petrologic types. Sample LAP 04462 exhibits the highest deviation of ~5%, which could indicate the presence of unequilibrated petrologic type 3 components among the lithic clasts entrained in this melt rock [*Van Schmus and Wood*, 1967]. Low-Ca pyroxenes are mostly orthorhombic, consistent with type 5 to 6 sources. Monoclinic crystals frequently occur together with microcrystalline pyroxene chondrule fragments in LAP 03922 and LAP 04751 (Figure 4a), suggesting a petrologic type 4 source for that debris [*Van Schmus and Wood*, 1967].

[18] Interstitial melt mesostasis was analyzed in clasts of all samples except LAP 02240, where the mesostasis was too small for microprobe analyses. Preserved melt mesostases in chondrules are consistent with type 4 material [*Van Schmus and Wood*, 1967]. Microcrystalline feldspar occurs in samples LAP 031308 and LAP 04751, and a single, 100 μm size clast of plagioclase is present in LAP 02240, which ought to indicate petrographic type 5 or 6 components. Only LAP 031125 lacks recognizable chondrule fragments but otherwise contains mostly well-crystallized single mineral clasts, which indicates a petrologic type 6 target source. All other samples contain fragments of type 4 to 5 chondrites (Figures 4a–4b) that are interpreted as their dominant target sources (Table 1). These are very tentative findings, given the limited amount of sample available, the variable amounts and sizes of lithic clasts, and the variable thermal and shock metamorphic overprints these clasts suffered.

[19] If these lithologies were excavated from primary thermal metamorphic source regions, then the thermal models of the H chondrite asteroid [*Bennett and McSween*, 1996] suggest LAP 031125 may contain material excavated from depths of at least 7 to 10 km; LAP 02240, 031175, 031308, and 04462 may contain material excavated from depths of at least 6 to 9 km; and LAP 03922 and 04751 may contain material excavated from depths of at least 4 to 6 km. For the oldest impact events (i.e., 3.9 Ga for LAP 02240 and 031125 [*Swindle et al.*, 2009]), these estimated depths are reasonable. For younger impact events (e.g., <1 Ga for LAP 03922, 031173, and 031308 [*Swindle et al.*, 2009]), after impact gardening may have created a megaregolith of mixed petrological components, or a rubble pile asteroid structure [*Michel et al.*, 2003; *Housen*, 2009], excavation depths for the thermally metamorphosed components may be significantly shallower.

3.4. Chemical Compositions and Microtextural Observations

3.4.1. Lithic Clasts

[20] Variable amounts of monomineralic and polymineralic lithic clasts ranging in size from ~15 μm to larger than the thin section scale are entrained in the impact melt. Most analyses of clast olivines ($Fa_{14–19}$, Tables 2 and A2) and low-Ca pyroxenes ($En_{81–87}Fs_{11–18}Wo_{0.4–3.4}$, Tables 2 and A3) fall in the range of compositions for H chondrites of $Fa_{16–20}$ and $Fs_{14.5–18}$ [*Brearley and Jones*, 1998]. High-Ca pyroxene (pigeonite, augite and diopside, Tables 2 and A4) was only found in the four samples that contain larger lithic clasts, where it is associated with microcrystalline pyroxene and radial pyroxene chondrule fragments. Melt mesostasis associated with chondrule clasts was found in all but one thin section and typically exhibits feldspathic affinities (Tables 2 and A5). Stoichiometric feldspar analy-

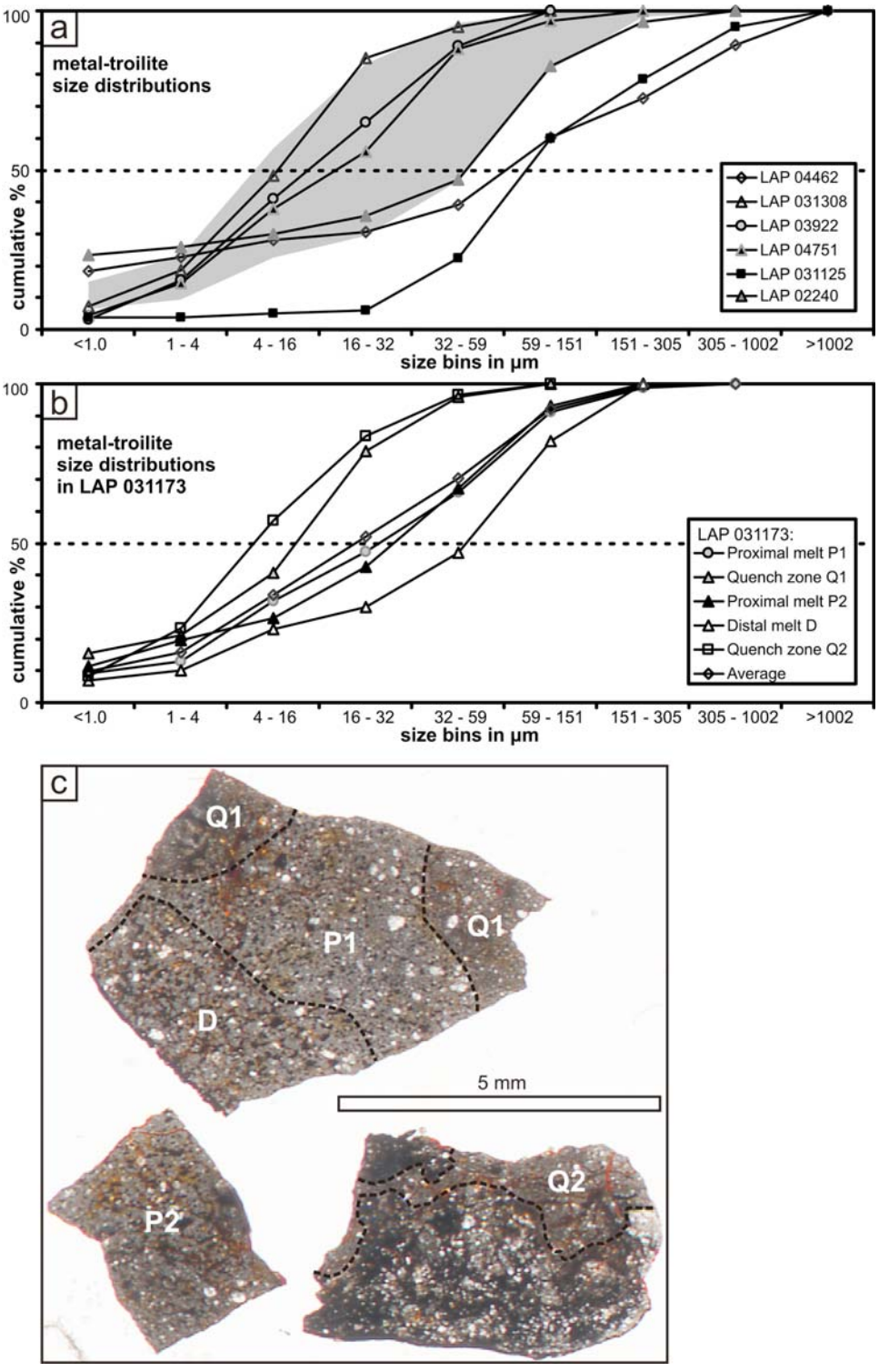

Figure 3. Metal and troilite size distributions. (a) Cumulative size distribution diagrams for the samples studied. The shaded area marks the range of size distributions captured in five separate areas analyzed in LAP 031173 and shown in Figure 3c. (b) Cumulative size distributions for five areas in LAP 031173 that are variably quenched melt zones around a mm size lithic clast and are shown in Figure 3c. (c) Thin section scan of LAP 031173. Hatched lines show the microscopically determined, approximate boundaries of melt zones with similar metal-troilite aggregate size distributions; Q1 and Q2 designate rapidly quenched melt zones, P1 and P2 are intermediately quenched melt zones, and D is the slowest quenched melt zone in this sample.

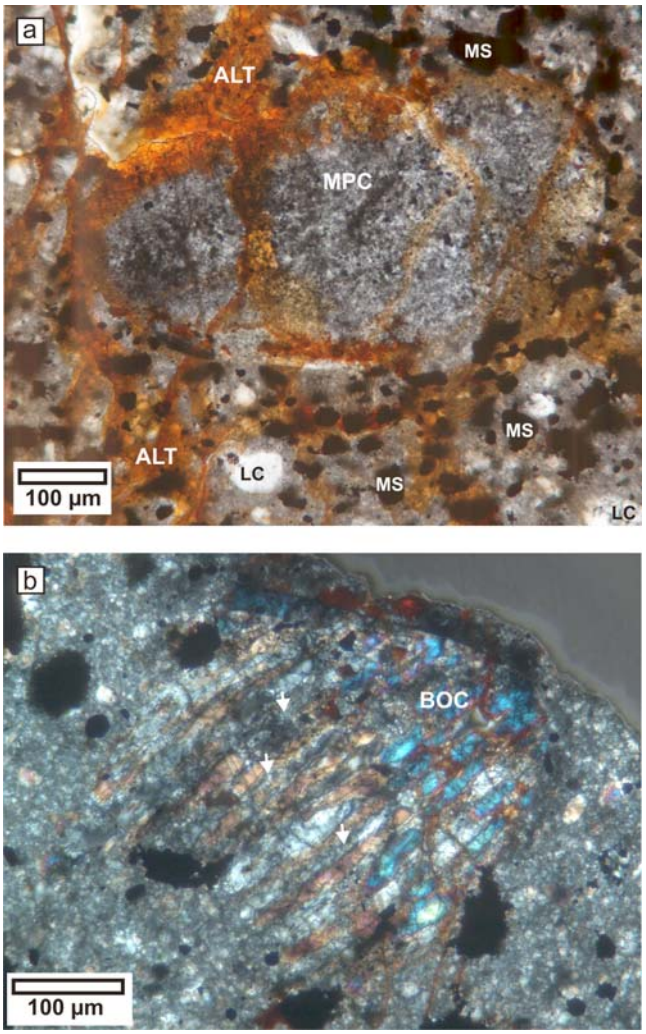

Figure 4. Chondrule fragments. (a) Microcrystalline pyroxene chondrule fragment (MPC) in LAP 03922 suggests type 4–5 source. Note surrounding impact melt with metal-sulfide aggregates (MS) and single-mineral lithic clasts (LC) and network of brown weathering zones (ALT). This chondrule type occurs in all samples except LAP 031125. Plane-polarized light micrograph. (b) Barred olivine chondrule fragment (BOC) in LAP 4462 with recrystallized matrix (arrows) suggests type 5 source. Cross-polarized light micrograph.

ses ($Ab_{83–86}An_{12–15}Or_{2–6}$) of lithic clasts were only produced from LAP 031308 and LAP 04751 (Table A5), indicating thermal metamorphic type 5 [*Van Schmus and Wood*, 1967]. Single clasts of olivine and low-Ca pyroxenes occur most frequently, while fragments of chondrules are less common. Chondrule fragments are more frequent in larger clasts that exhibit intense brittle deformation (Figure 5). Undulous extinction, mosaicism (Figure 6) and planar fractures in olivine and low-Ca pyroxene are ubiquitous shock metamorphic features but no high-pressure polymorphs were recognized. Moreover, olivine and low-Ca pyroxene frequently exhibit submicron size metal and sulfide injections that sometimes display alignment. More extreme examples with a high density of such injections appear shock blackened on the microscopic scale. Sulfide and metal were found to be concentrated in coarse, mm thick veins in some shock-blackened, larger lithic clasts (Figure 5). Occasionally, Fe-Ni metal and sulfide form mm thick agglomerates at the interface of larger lithic clasts with the silicate impact melt.

3.4.2. Impact Melt

[21] Impact melt is densely crystallized with <10 μm size phenocrysts of olivine ($Fa_{13–18}$; Tables 2 and A6) and low-Ca pyroxene ($En_{81–87}Fs_{11–17}Wo_{0.4–3.8}$, Tables 2 and A7) that are concentrically zoned with Mg-rich cores and Fe-rich rims. A feldspathic mesostasis $Na_{18–24}Ca_{70–77}K_{5–6}$ in LAP 02240 and LAP 04751, and $Na_{61–73}Ca_{14–31}K_{8–14}$ in LAP 04462, LAP 03922, and LAP 031125, (Table 2) fills interstitial spaces and is typically continuous over 2–5 μm domains (Figure 7). These domains are too small to produce reliable chemical analyses with the microprobe, because they are comparable to the excitation diameter of the electron beam, so no microprobe data are reported.

3.4.3. Fe-Ni Metal and Troilite

[22] The impact melt contains characteristic droplets of immiscible sulfide and Fe-Ni metal (Figure 8). Their shapes range from circular to strongly elongated vermicular and their alignment occasionally records a flow texture. Fe-Ni metal is generally zoned with U-shaped Ni-concentration patterns across the particles. No secondary kamacite rims were observed. The results for the measurement traverses are summarized in Table 3. All but one metal particle indicate phosphorous saturation with P concentrations $\geq$ 0.1 wt % [*Smith and Goldstein*, 1977], yet no phosphide minerals were detected. Troilite crystals have variable Ni contents (Table 3) that indicate rapid quenching [*Smith and Goldstein*, 1977], but concentrations of Ni above a few wt % were considered mixture analyses with metal.

[23] Calculated cooling rates for the period of thermal equilibration between the melts and clast-melt mixtures were between 0.8 and 39.5°C/s (Table 4), as determined according to the method of *Scott* [1982]. For Orvinio, a stage 1 cooling rate of ~5°C/s was found, which falls in the typical range of the other samples studied (Figure 9).

4. Discussion

4.1. Crystallization and Silicate Metal Differentiation

[24] In all the samples studied, the impact melts began to crystallize, producing ultramafic olivine-pyroxene assemblages in residual feldspathic mesostases that are enriched in the moderately and highly incompatible elements that would constitute feldspars (SiO_2, Al_2O_3, Na_2O and K_2O; Table 2; compare *Fodor and Keil* [1976a]). Olivine and pyroxene crystals that grew from the impact melt are compositionally zoned, indicating typical liquidus evolution toward an increase in Fe content. Still, most analyses fall within the range of olivines and pyroxenes in associated lithic clasts and are a good match for typical H chondrites (Table A4) [*Brearley and Jones*, 1998]. Thus, there is no major element indication that projectiles significantly perturbed the melt compositions.

[25] Metal in the melts crystallized as taenite and martensite (Table 3), rather than the kamacite found in the target materials. For that reason, it is impossible to use standard minor element indicators (i.e., the Co concentration in

Table 2. Summary of Silicate Analyses[a]

		Olivine	Low-Ca Pyroxene			High-Ca Pyroxene			Melt Mesostasis			
Sample Thin Section	Lithology	Fa	En	Fs	Wo	En	Fs	Wo	Na	Ca	K	SiO_2 (wt %)
LAP 02240, 8	clasts	15–18	83–85	13–16	1–3	ND	ND	ND	NR	NR	NR	NR
	matrix	14–17	83–87	11–15	0.4–2	ND	ND	ND	13–22	72–81	5–7	53–67
LAP 03922, 6	clasts	16–18	81–84	14–17	1–2	57–80	9–15	5–34	62–83	16–30	1–10	61–72
	matrix	13–18	83–84	15–16	1	ND	ND	ND	42–65	23–49[b]	10–13[b]	56–67[b]
LAP 04751, 6	clasts	17–18	80–85	14–18	1–3	48–80	5–17	6–46	97–98	0–0.4	2	64–65
	matrix	17–18	83–85	14–15	1	ND	ND	ND	20–24	70–74	5–6	57–64
LAP 031125, 4	clasts	15–18	82–88	11–16	1–3	ND	ND	ND	26–78	9–38	11–37	73–76
	matrix	16–18	84–87	12–15	1	ND	ND	ND	63–73	14–26	11–14	70–74
LAP 031173, 6	clasts	17–18	82–86	11–16	1–2	48–49	5	46–47	53–84	13–40	2–7	62–67
	matrix	16–18	82–84	15	1–3	ND	ND	ND	42[c]	49[c]	10[c]	67[c]
LAP 031308, 4	clasts	17–19	82–84	15–16	1–2	48–53	5–7	41–47	59–88	10–32	2–11	60–72
	matrix	16–18	81–83	15–17	1–4	ND	ND	ND	NR	NR	NR	NR
LAP 04462, 8	clasts	14–19	82–87	12–17	0.35–3	ND	ND	ND	35[c]	16[c]	5[c]	61[c]
	matrix	15–17	83–87	12–15	1–3	ND	ND	ND	61–64	26–31	8–10	71

[a]ND, none detected; NR, no reliable analysis. Values are mole ratios.
[b]Three analyses with poor totals.
[c]One reliable analysis.

kamacite) to determine if the metal has a wholly H chondrite affinity, too. Although a contribution of a projectile component to the siderophile budget cannot be ruled out, it is limited to ~1 wt % of the siderophiles or ~0.2 wt % of the bulk melt, because the modal contents of Fe-Ni metal and troilite in the samples fall within the normative range of H chondrites (Table 1) [*Mason*, 1965; *McSween et al.*, 1991]. The one exception is LAP 031125, for which the modal compositional data indicates strong depletion in Fe-Ni metal plus troilite compared to the typical range of H chondrites. This depletion coincides with the slowest stage 1 cooling rate in all the samples studied (Table 4), suggesting there was sufficient time for the agglomeration of Fe-Ni metal and troilite and, thus, separation of siderophile from lithophile components in the cooling impact melt.

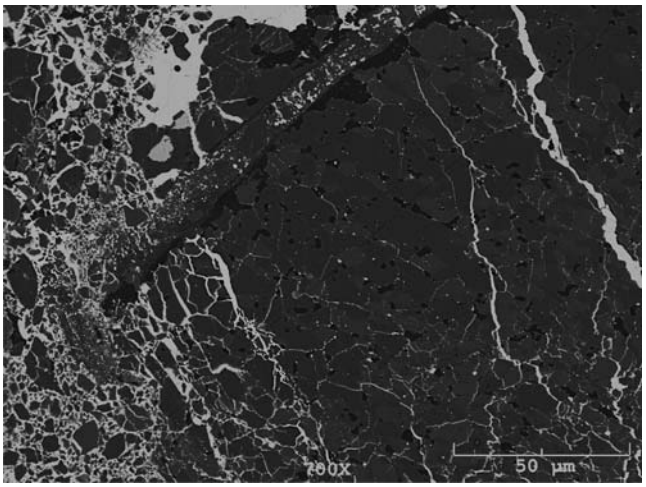

Figure 5. Large lithic clasts. Chondrule fragment of microcrystalline pyroxene with interstitial plagioclase that is part of a large, shock-blackened lithic breccia clast in LAP 04751. Bright veins are troilite metal that also overprints the breccia matrix. Scanning electron microscopy (SEM) backscattered electron (BSE) image.

4.2. Impact Melts Similar to the LAP Samples

[26] Hints of similar types of agglomeration and segregation have been discerned from clasts of impact melt in chondritic breccias. *Leitch and Grossman* [1977] described a 2.1 mm long clast in the shocked H6 breccia Supuhee. The clast has a fine-grained silicate matrix and oriented, up to 130 μm long inclusions of Fe-Ni metal and troilite. More importantly, while the silicate melt matrix composition is consistent with an H chondritic composition, the bulk clast is depleted in troilite and metal.

[27] Not all melt clasts in H chondritic breccias, however, have this metal-sulfide depletion.

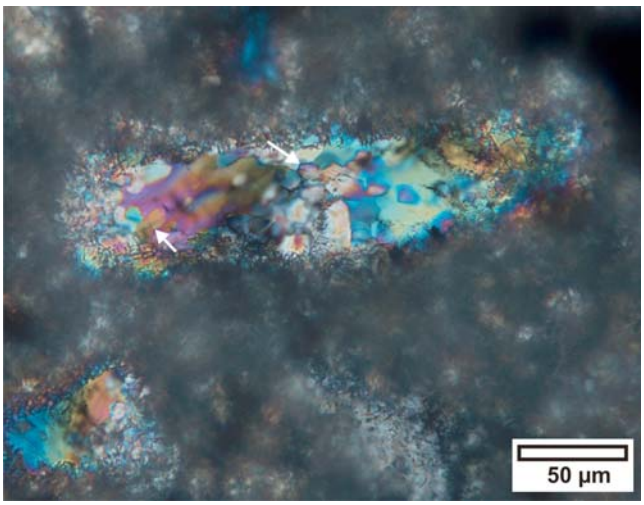

Figure 6. Shock-induced mosaicism and resorption of lithic clast. Olivine clast that exhibits marginal resorption and pronounced shock mosaicism (arrows) in impact melt of LAP 031125. Such strong mosaicism is indicative of shock pressures between 30 and 55 GPa and a post shock temperature increase of 250°C –850°C (shock stage S5) [*Stöffler et al.*, 1991], which likely promoted resorption. Cross-polarized light micrograph.

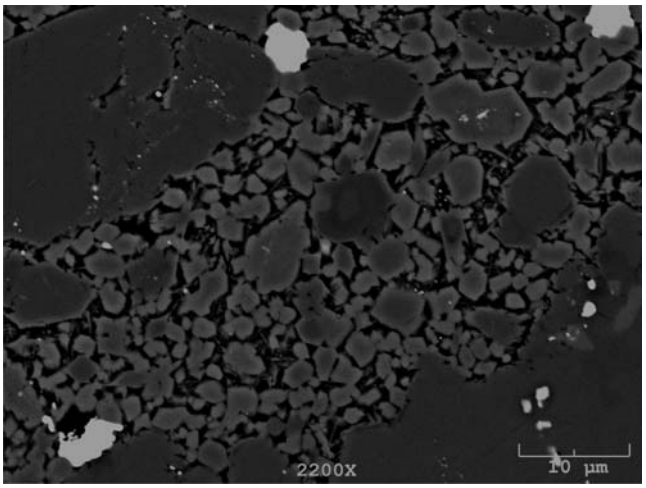

Figure 7. Impact melt matrix. Zoned, euhedral olivine (bright gray) and low-Ca pyroxene (dark gray) crystals in a feldspathic melt mesostasis (black) constitute the silicate impact melt in LAP 04751. White phases are Fe-Ni metal or troilite. SEM-BSE image.

[28] *Fodor et al.* [1980] describe a 1 cm size impact melt fragment in the H5 chondrite Adams County, Colorado. This exotic melt fragment was impact reworked and incorporated into the H5 chondrite after equilibration of its host. Therefore, although the matrix of its host is recrystallized, the melt rock clast retains a glassy melt mesostasis. Textures, phenocryst sizes, and martensitic compositions of metal particles in this clast-rich impact melt particle closely resemble the seven LAP samples investigated in this study.

4.3. Melt Cooling Rates and Their Geologic Contexts

4.3.1. Quenching of the LAP Samples and Orvinio

[29] Comparison with the cooling rates derived from rapidly solidified Fe-FeS globules (Figure 9) [*Scott*, 1982] suggests the stage 1 cooling rates of the samples in this study are similar to those of clasts in the H chondrite breccias Weston, Pulsora and Tysnes Island, which were interpreted to having solidified due to radiative cooling before meteorite compaction. The Yanzhuang H chondrite [*Ming et al.*, 1995] contains melt pockets that initially cooled at 6 to 30°C/s, similar to Orvinio and the LAP samples (Table 4). However, more rapid quenching due to conductive heat transfer was determined for melt veins that cooled in the same stage 1 temperature interval at 100 to 400°C/s (Figure 9) [*Ming et al.*, 1995; *Kring et al.*, 1996]. *Scott* [1982] interprets metal globules with cooling rates of 1–300°C/s as components inside hot silicate melt volumes with diameters between 6 and 40 mm on or near the surface of their parent asteroid. These melt volumes roughly agree with the sample dimensions and the observed amounts of melt in the meteorite specimen (Figures 1a–1f) and their thin sections (Figures 2a–2b).

[30] Stage 1 cooling of the LAP samples was dominated by the thermal equilibration of superheated impact melt and relatively cool clasts (Figure 3). Afterward, the clast-rich impact melts cooled radiatively or conductively to their surroundings. The second stage of the cooling process can be slower and can occur over longer time. If the melt cools sufficiently slow, then Fe-Ni diffusion in the metal will produce secondary rims of kamacite. The diffusional profiles and thicknesses of these kamacite rims can be used to quantify stage 2 cooling [*Smith and Goldstein*, 1977; *Taylor et al.*, 1979; *Kring et al.*, 1996].

[31] Stage 2 cooling rates in the seven LAP impact melts were too fast to allow the growth of kamacite (Table 3). Consequently, after thermal equilibration, cooling rates were faster than ~5°C/a (1.6×10^{-7}°C/s) and burial depths <100 m [*Smith and Goldstein*, 1977] (see Appendix A).

[32] Although the metal globules are not surrounded by secondary kamacite, they are chemically zoned. Examples of these types of Ni-Fe gradients in metal globules have been produced experimentally for the Ramsdorf L chondrite impact melt and used to produce semiquantitative cooling rates for Orvinio [*Smith and Goldstein*, 1977]. Ramsdorf has steep Ni gradients from 8 to 20 wt % and a high Ni content (0.11 wt %) in adjacent troilite. Based on their experimental calibration, *Smith and Goldstein* [1977] inferred a cooling rate of 10^{-3}°C/s. Orvinio has metal globules with slightly smaller Ni gradients of 1 to 8 wt % that are adjacent to troilite with 0.08 wt % Ni, from which *Smith and Goldstein* [1977] inferred a stage 2 cooling rate of 10^{-3} to 10^{-4}°C/s. All LAP samples exhibit troilite with variable but generally substantiative Ni concentrations and taenite-martensite gradients between ~2 and 10 wt % (Table 3). Following *Smith and Goldstein* [1977], while the rim gradients seem to match those of Orvinio, the Ni concentrations in troilite suggest a similarity to those of the experimentally heat treated globules of Ramsdorf that were found to contain Ni concentrations between 6.05 and 0.15 wt % after quenching at cooling rates of 10^{-2} to 10^{-3}°C/s from temperatures of 1050 to 1200°C. From this similarity (Table 4), stage 2 cooling rates on the order of 10^{-2}–10^{-3}°C/s are approximated for the LAP samples. An independent indicator for rapid cooling in all samples studied is the high nucleation rate and slow growth of olivine and pyroxene phenocrysts in

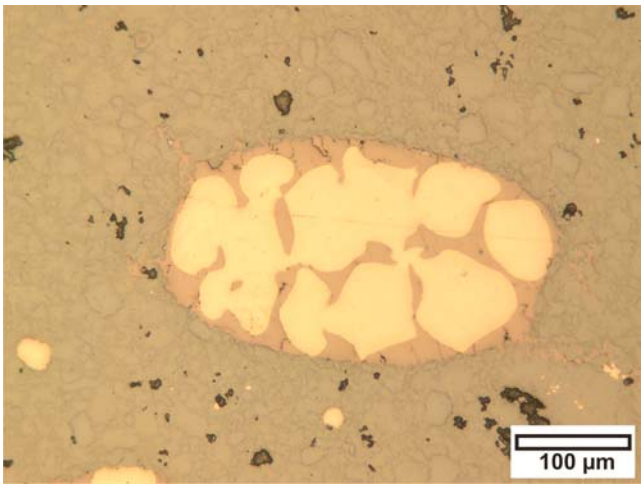

Figure 8. Fe-Ni metal and troilite globule. Globule of troilite enclosing bright Fe-Ni metal droplets in the silicate impact melt of LAP 04462. Reflected light image.

Table 3. Summary of Fe-Ni Metal and Troilite Analyses[a]

			Metal			Martensite			Taenite Maximum Concentration		Ni in Troilite	
Thin Section	Type	Name	Width (μm)	Mean P (wt %)	Mean Co (wt %)	Width (μm)	Mean Ni Weight Percent	σ	Ni (wt %)	Co (wt %)	Minimum (wt %)	Maximum (wt %)
LAP 04462, 8	globule	M5	98	0.22	0.39	60	6.36	0.22	11.13	0.41	0.09	0.13
LAP 04462, 8	globule	M4	64	0.26	0.45	48	8.54	0.13	11.6	0.45	0.04	1.75
LAP 04462, 8	globule	M1	108	0.17	0.46	74	6.36	0.15	12.99	0.47	0.03	0.1
LAP 04462, 8	globule	M3	82	0.41	0.43	74	7.5	0.73	11.83	0.47	0.01	0.4
LAP 04751, 6	globule	M-E	74	0.13	0.48	62	6.53	0.2	8.25	0.52	0.16	7.51
LAP 04751, 6	globule	M-D	52	0.41	0.44	30	7.41	0.11	11.65	0.52	0.16	0.66
LAP 04751, 6	globule	M-B	186	0.1	0.49	82	6.96	0.07	11.48	0.49	0.08	0.5
LAP 031125, 4	globule	M-B	120	0.52	0.43	106	7.83	0.45	13.11	0.47	0.02	0.23
LAP 031125, 4	globule	M-A	160	0.35	0.42	124	7.41	0.68	11.78	0.48	0.03	0.38
LAP 031125, 4	globule	M-C	90	0.52	0.44	70	8.41	0.12	12.74	0.45	0.03	0.17
LAP 031308, 4	clast	M6	171	0.07	0.49	98	6.92	0.19	9.75	0.47	NA	NA
LAP 031308, 4	globule	M5	42	0.4	0.47	33	7.26	0.71	17.66	0.51	0.48	1.57
LAP 031308, 4	globule	M4	82	0.25	0.47	80	7.92	0.75	11.57	0.52	0.09	0.47
LAP 03922, 6	globule	M1a	114	0.13	0.47	84	6.74	0.15	9.78	0.51	0.03	1.33
LAP 03922, 6	globule	M1b	81	0.2	0.46	76	7.28	0.51	15.08	0.48	0.14	0.19
LAP 03922, 6	globule	M2	33	0.28	0.48	24	6.17	0.26	11.25	0.51	0.1	0.14
LAP 03922, 6	globule	M3	46	0.21	0.49	38	6.79	0.13	8.76	0.41	0.16	NA
LAP 03922, 6	clast	M4	32	0.24	0.35	29	9.54	0.67	14.07	0.42	0.1	1.42
LAP 031173, 6	clast	M6a	50	0.14	0.48	41	7.25	0.37	9.69	0.46	0.31	1.16
LAP 031173, 6	clast	M6b	11	0.27	0.42	NA	9.01	0.11	13.88	0.42	0.31	0.35
LAP 031173, 6	globule	M6c	52	0.43	0.44	48	7.6	0.64	9.59	0.41	NA	NA
LAP 031173, 6	globule	M6d	28	0.4	0.45	22	8.39	0.19	13.15	0.47	0.26	0.28
LAP 031173, 6	globule	M5	48	0.31	0.43	45	7.6	0.62	12.93	0.51	0.2	0.43[b]
LAP 031173, 6	globule	M4	49	0.27	0.46	45	7.37	0.59	9.77	0.44	0.2	ND[b]
LAP 031173, 6	globule	M3	37	0.23	0.5	23	6.15	0.19	8.44	0.44	0.15	1.16
LAP 031173, 6	globule	M2	90	0.26	0.47	80	7.81	0.78	16.84	0.57	0.71	NA
LAP 031173, 6	globule	M1	49	0.38	0.46	45	7.46	0.77	15.05	0.45	0.24	1.3
LAP 02240, 8	globule	M-A	38	0.4	0.4	34	7.6	0.24	10.98	0.4	0.84[c]	0.84[c]
LAP 02240, 8	globule	M-B	22	0.39	0.39	18	8.36	0.42	11.03	0.45	0.97[c]	0.97[c]
LAP 02240, 8	globule	M-C	52	0.44	0.38	46	7.91	0.1	9.64	0.43	0.31	1.35
LAP 02240, 8	globule	M-D	14	0.41	0.38	6	7.45	0.26	9.47	0.38	0.17	0.53
LAP 02240, 8	clast	M-E	30	0.41	0.39	20	8.43	0.17	12.16	0.41	0.26	0.5
LAP 02240, 8	clast	M-F	52	0.49	0.4	36	8.29	0.34	10.86	0.42	0.32	0.36
LAP 02240, 8	clast	M-G	52	0.52	0.42	42	8.36	0.26	12.11	0.47	0.27	0.35

[a]NA, not analyzed; ND, none detected; concentrations of S, Mg, Si, Ca, Mn, Cr, Cu, Ti, V, Zn were typically at or below the limit of detection (~0.01 wt %); totals were 98.5–101.5 wt % but occasionally, totals as low as 97 wt % were accepted for the measurement points with the highest Ni contents because such points may have been at the metal-troilite interface or close to a void.
[b]Poor totals.
[c]Single measurement.

the glassy melt matrix that resulted from pronounced undercooling [*Winter*, 2001].

4.3.2. Cooling Characteristics of Other H Chondrite Impact Melts

[33] In contrast to the seven LAP samples and Orvinio, the clast-rich impact melt Rose City indicates cooling at ~0.03°C/s through the temperature interval between ~1400 and 950°C [*Scott*, 1982]. It also crystallized secondary kamacite at temperatures between ~700 and 400°C, during slow stage 2 cooling on the order of ~0.4°C/a (1.2E–8°C/s) at a burial depth of ~200 m in an impact breccia lens on the H chondrite asteroid (see Appendix A and *Smith and Goldstein* [1977]).

Table 4. Stage 1 Cooling Rates

		Average Globule Spacing		Stage 1 Cooling Rate[a]			
Sample	Metal-Troilite Globules	Mean (μm)	Maximum (μm)	Mean (°C/s)	Minimum (°C/s)	Maximum (°C/s)	Diameter Melt Sphere[b] (mm)
LAP 02240	12	39.1	160	12.8	8.5	27.6	9
LAP 04751	18	28.0	230	34.1	19.2	67.8	5
LAP 03922	18	26.5	144	39.5	11.2	170.7	5
LAP 04462	43	66.4	225	2.8	1.4	7.1	19
LAP 031125	29	103.8	220	0.8	0.4	1.6	37
LAP 031173	18	35.8	175	16.6	8.5	30.4	8
LAP 031308	10	29.6	260	28.7	11.2	121.3	6
Orvinio	83	55.0	75	4.8	1.9	12.0	15

[a]Stage 1 cooling rate calculations: $R = 530000 \times d^{-2.9}$, with (d) the distance between metal globules and R in (°C/s).
[b]Diameters of melt spheres were calculated according to the equation $\log R = -0.5 \log C - 1.8$ with R = radius of the melt sphere in (m) and C, the average stage 1 cooling rate in (°C/s).

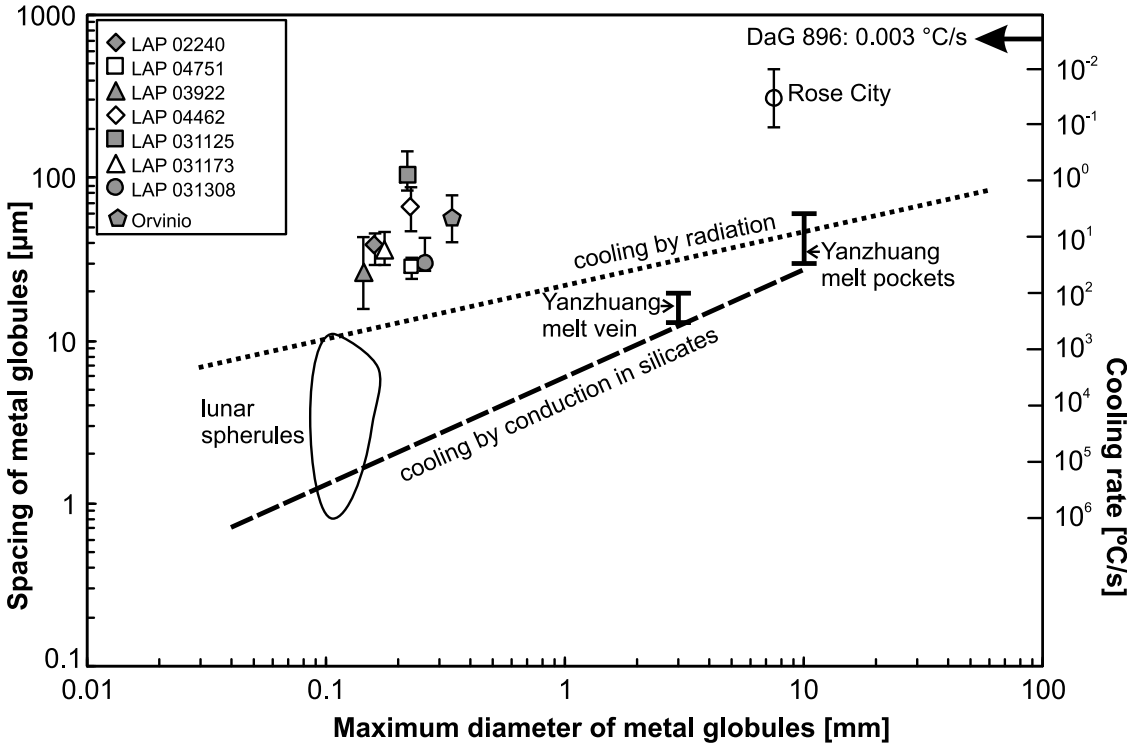

Figure 9. Spacing of metal globules versus maximum diameter of metal globules that formed by impact melting of chondritic material after *Scott* [1982]. Cooling in cold regolith is approximated by the field of lunar spherules. Cooling rates close to those typical for conduction in silicates suggests injection in much colder material. Data for Yanzhuang from *Ming et al.* [1995] and Dar al Gani 896 from *Folco et al.* [2004].

[34] The H chondrite impact melt Dar al Gani (DaG) 896 is almost devoid of Fe-Ni metal and crystallized up to 1 mm size olivine phenocrysts, 2 orders of magnitude larger than the phenocrysts in the seven LAP samples. Based on thermodynamic crystallization modeling, a cooling rate through the temperature interval between ~1630 and 1300°C of ~0.003°C/s was inferred for DaG 896 [*Folco et al.*, 2004]. This is several orders of magnitude slower than the seven LAP samples (Figure 8). For DaG 896, these authors suggest a setting as a melt dike or a differentiated melt body at the bottom of a breccia lens on the H chondrite asteroid. As a note of caution, the different methods used to determine the stage 1 cooling of DaG 896 and Rose City may limit their direct comparability.

[35] Several metal- and troilite-deficient H chondrite impact melt fragments that are petrographically similar to DaG 896 were described in H chondrite breccias: A melt clast in Ourique exhibits ~300 μm size phenocrysts [*Kring et al.*, 2000]; an inclusion in Yamato 794046 crystallized ~2 mm size phenocrysts [*Sack et al.*, 1994]; and a melt clast in Northwest Africa (NWA) 2457 displays ~500 μm size phenocrysts [*Fernandes et al.*, 2006; V. A. Fernandes, personal communication, 2009]. Because these melts are clasts in H chondrite breccias, they likely indicate excavation and reworking by impact(s) prior to ejection from the parent asteroid.

4.3.3. Terrestrial Analogs

[36] Interpretations of chondritic impact melt rocks frequently invoke injections of melt into dikes in crater floors [e.g., *Stöffler et al.*, 1991; *Keil et al.*, 1997; *Folco et al.*, 2004]. Comparison with terrestrial impact craters indicates that meter size melt dikes in crater floors are related to voluminous overlying melt sheets, whereas clast-rich impact melt rocks form at the interface of melt sheets with suevite [*Grieve et al.*, 1977] or as pods in suevite deposits, e.g., at the 3.8 km diameter simple crater Brent [*Grieve*, 1978]. An analogy to pseudotachylites is unrealistic because troilite and metal segregation would not be expected to happen in pseudotachylitic melts [*Dressler and Reimold*, 2004]. Melt-dike emplacement at the >200 km multiring impact basins Sudbury and Vredefort on Earth is linked to large-scale crater collapse [*Thompson and Spray*, 1994] and massive melt sheets, which are implausible scenarios for the H chondrite parent asteroid [*Keil et al.*, 1997]. In summary, the comparison with melt distribution in terrestrial impact structures would imply that melt dikes on an asteroid occur together with impact melt sheets or discontinuous pods of impact melt several orders of magnitude larger in volume [*Grieve*, 1978; *Dressler and Reimold*, 2001]. Thus, metal-troilite-deficient H chondrite impact melt rocks that solidified at cooling rates slower than ~10^{-2}°C/s (Figure 9) more likely formed in larger melt pods or discontinuous melt sheets in breccia lenses of large simple craters, possibly analogous to Brent [*Grieve*, 1978]. Extrapolating to the seven LAP samples and Orvinio, these melts record rapid, radiation-dominated cooling. This suggests they were parts of small, near-surface melt volumes in simple craters on the H chondrite asteroid.

4.4. Cratering on the H Chondrite Asteroid

[37] The seven H chondrite impact melt specimens (Tables 1–4) are part of a growing number of meteorites that can be used to reconstruct the collisional evolution of the H chondrite parent asteroid and fragments generated from it.

4.4.1. Early Disturbance

[38] One of the earliest collisional events on the H chondrite asteroid is represented by the Portales Valley metallic melt breccia, which has an Ar-Ar closure age of ~4465 Ma [*Bogard and Garrison*, 2009]. Taking into account the slow metallographic cooling rate of ~6.5°C/Ma [*Sepp et al.*, 2001] recorded in this meteorite, and a closure temperature for the Ar-Ar system at ~240°C [*Turner et al.*, 1978], the Ar-Ar age of ~4465 Ga was only attained >40 Ma after cooling of the metal veins through the temperature interval between ~700 and 400°C. This implies Portales Valley formed on the H chondrite parent asteroid during cooling from peak metamorphic temperatures [*Ruzicka et al.*, 2005; *Bogard and Garrison*, 2009] in an impact cratering event for which *Kring et al.* [1999] inferred a minimum diameter of 20 km.

[39] More dramatic events have been inferred for that same time interval. Shattering and/or disruption of the H chondrite parent asteroid were proposed to explain an apparent discrepancy between thermal metamorphic grade and metallographic cooling rates in certain meteorites [*Grimm*, 1985; *Taylor et al.* 1987; *Grimm et al.*, 2005]. Disruption and almost instantaneous reassembly of the H chondrite parent asteroid require very large projectiles and the production of a substantial amount of impact melt. For a collisional disruption event of a 200 km diameter asteroid, *Keil et al.* [1997] calculated a volume of impact melt on the order of 9400 km^3. There is little evidence of such large volumes of impact melt with such old ages. This disruption model is also at odds with evidence from U-Pb dating [*Göpel et al.*, 1994], Pu-fission track- and Ar-Ar dating [*Trieloff et al.*, 2003], and Hf-W thermochronometric modeling [*Kleine et al.*, 2008], which are consistent with largely intact series of concentric zones of progressive metamorphic grade toward the core on their parent asteroid. Similarly, *Schwarz et al.* [2006] conclude that all thermochronological data for H chondrites are consistent with simple cooling of a large asteroid that suffered several impacts on its surface during the first ~60 to 100 Ma of its existence. It is thus inferred that the H chondrite parent asteroid survived collisional growth of planetesimals after runaway accretion [*Bottke et al.*, 2005] fairly intact.

4.4.2. Ancient Impacts

[40] Nonetheless, ancient cratering events on the H chondrite asteroid before 4200 Ma are recorded by melt rock clasts in Dhofar 323 at 4508 ± 9 Ma [*Korochantseva et al.*, 2008], NWA 2457 at 4503 ± 12 Ma [*Fernandes et al.*, 2006], Ourique at 4410 ± 20 Ma [*Kring et al.*, 2000] or 4360 ± 120 Ma [*Swindle et al.*, 2009], and with Portales Valley before 4465 ± 23 Ma (see previous discussion and *Bogard and Garrison* [2009]). This cluster means that in this era, at least one large crater with a diameter >20 km formed on the H chondrite asteroid. The floor of this crater contains segregated metal and troilite veins through brecciated silicate as recorded in the Portales Valley meteorite [*Kring et al.*, 1999]. Moreover, impact melt volumes differentiated metal troilite from silicate portions, which have since been obliterated and incorporated as clasts in Dhofar 323, Ourique, and NWA 2457. Scaling relationships [*Holsapple et al.*, 2002] and numerical simulations [*Michel et al.*, 2003; *Housen*, 2009] suggest that an impact that produced a >20 km wide crater on a 90 to 200 km diameter asteroid severely degraded the integrity of its target, predisposing it to later disruption.

4.4.3. Continuous Large Collisions Until ~3600 Ma

[41] Between 3600 and 4100 Ma several impact cratering events formed melts, including LAP 02240 at ~3939 ± 62 Ma and LAP 031125 at 3942 ± 23 Ma. Based on a combination of cosmogenic nuclides, petrography and ^{40}Ar-^{39}Ar systematics, *Swindle et al.* [2009] concluded that these samples are unlikely to be paired, although pairing is always difficult to rule out definitively. Also, these events are of poorly constrained magnitude. However, at least one impact in this era was large enough to produce metal and troilite segregation from silicate. This was recorded with DaG 896 at ~3704 ± 35 Ma [*Folco et al.*, 2004], in an igneous inclusion in Yamato-79046 at 3790 ± 40 Ma [*Fujimaki et al.*, 1994], and with a strongly crystallized clast in the Plainview meteorite [*Fodor and Keil*, 1976b] at 3630 ± 70 Ma [*Keil et al.*, 1980]. An impact at 3620 ± 10 Ma [*Kunz et al.*, 1997] produced a crater that hosted the slowly cooled Rose City melt rock [*Smith and Goldstein*, 1977]. A minimum size for the crater that contained Rose City can be derived from scaling relationships, assuming the maximum breccia fill is approximately half the true depth of a simple crater [*Grieve*, 1987]. If the ~200 m burial depth for Rose City (see Appendix A) is taken as the minimum depth of the thickness of the crater fill breccia, then that burial depth implies a crater ~200 m deep [*Grieve*, 1987]. A minimum diameter for this crater of 1 to 1.4 km can then be estimated if the (observed) depth-to-diameter ratios for small asteroids and the Moon of 1:5 to 1:7 are applied [*Sullivan et al.*, 1996]. The ages of the seven LAP meteorites are sufficiently disparate that they represent multiple impact events. The data are consistent with a lunar and inner solar system cataclysm [*Turner et al.*, 1973; *Tera et al.*, 1974; *Bogard*, 1995; *Kring and Cohen*, 2002] but the number of meteorites analyzed thus far is too small to determine if this represents a dramatic increase in the impact flux.

4.4.4. Decreased Collisional Intensity

[42] There then seems to be a lull in significant impact activity between ~3600 and ~1500 Ma. *Swindle et al.* [2009] report several events at ~1400 Ma, ~900 Ma, and 300–600 Ma from the rapidly quenched, clast-rich melt rocks Gao Guenie, LAP 03922, LAP 031125, LAP 031308, Orvinio, and NWA 2058. Disturbed K-Ar systematics indicative of impacts during this time span have also been found in the shock-veined H chondrites Charsonville [*Grady*, 2000], Jilin, and Travis County [*Stöffler et al.*, 1991], Kimble County [*van der Bogert et al.*, 2003] and the strongly shocked H chondrites Dimmit [*Stöffler et al.*, 1991] and Monroe [*Britt and Pieters*, 1994], the host of Rose City [*Bogard et al.*, 1976], the moderately shocked and reheated chondrite Sweetwater [*Bogard et al.*, 1976] and Tulia [*Grady*, 2000], for which no melting is reported. Overall, it is intriguing to note that these samples do not record the production of larger impact melt volumes, and thus larger cratering events, after ~3600 Ma.

4.4.5. Youngest Collisions

[43] Cosmic ray exposure ages [*Graf and Marti*, 1995] reflect the youngest impact events on the remains of the H chondrite parent asteroid, some of which ejected the H chondrites that currently reach Earth. *Benoit and Sears* [1992] inferred a breakup event of the H chondrite asteroid 8 Ma ago, based on cosmic ray exposure ages, thermoluminescence properties and size distributions of Antarctic meteorites. However, compared to the widespread isotopic resetting and production of melt rocks from the L chondrite parent asteroid some 500 Ma ago, a similar signal does not show up with H chondrites [*Keil et al.*, 1994; *Swindle et al.*, 2009]. On average, H chondrites record relative lower degrees of shock metamorphic overprints than L and LL chondrites [*Lipschutz and Schultz*, 2007]. Also, petrologic type 5 material is overrepresented among the H chondrites [*Grady*, 2000] compared to the relative proportion of this material in thermal models of the H chondrite asteroid. According to the thermal models of *Bennett and McSween* [1996], type 5 petrologic material is expected to represent the smallest, and type 6 petrologic material by far the largest volume of the H chondrite parent asteroid. Catastrophic disruption therefore ought to produce a statistical sample of all petrologic types with a main mass of type 6 material, which is the case for L and LL chondrites [*Grady*, 2000; *Lipschutz and Schultz*, 2007]. A sample bias could be due to derivation of H5 material from a specific fragment or region of the H chondrite parent asteroid, as is suggested by CRE ages and fall times for H5 chondrites [*Graf and Marti*, 1995].

[44] On the other hand, it is also possible that the nature of the breakup events and the fragmentation of the parent asteroids varied. As noted in the introduction, cosmogenic exposure ages suggest the H chondrite parent asteroid, or a fragment of it, was affected by multiple collisional events over the past 100 Ma, including events ~60, ~33, and ~8 Ma ago. Furthermore, there is a trace element hint that a km size H chondrite fragment hit the Earth ~73 Ma to produce the Lappajärvi crater [*Tagle et al.*, 2007]. These data suggest the H chondrite parent asteroid was involved in several collisional events that ejected material, rather than a single, much larger disruption event.

[45] Two asteroids larger than ~100 km diameter have been disrupted in the main belt during the last ~100 Ma. These disruption events produced the Veritas asteroid family at 8.3 ± 0.5 Ma, and the Brasilia family at 50 ± 40 Ma [*Nesvorný et al.*, 2005]. If the 8 Ma cosmogenic ages reflect the disruption of the H chondrite parent asteroid, then Veritas may be the preferred source. Alternatively, following *Farley et al.* [2006], Brasilia or Veritas debris may have impacted what remained of the H chondrite asteroid ~8 Ma ago and generated debris that evolved into Earth-crossing orbits.

5. Implications

[46] 1. Petrologic and chronologic data indicates that differentiated, more slowly cooled impact melts only formed before ~3600 Ma on the H chondrite parent asteroid and were since reworked and incorporated into polymict breccias. If this inference holds true, then no large impacts affected the H chondrite parent asteroid past ~3600 Ma, or records of such large impacts were not excavated, ejected, and delivered to Earth. This could translate to a disruption event at around that time, which may have produced a rubble pile asteroid, an asteroid family, or a large remnant asteroid fragment. Disruption due to strength degradation from cumulative impact damage [*Gault and Wedekind*, 1969; *Michel et al.*, 2003; *Housen*, 2009] would be expected as a result from earlier, near-shattering impacts on the H chondrite parent asteroid. The smaller-sized remains of the H chondrite asteroid may not have been able to sustain impacts that produce larger melt volumes, where metal and troilite differentiated from silicates. A minimum size for such craters ought to be on the order of km in diameter, somewhat similar to the presumed size for the crater that hosted the slowly cooled but undifferentiated Rose City melt rock. The present state of the H chondrite parent object remains unresolved, because, unlike L chondrites, Ar-Ar ages of H chondrites do not indicate a severe degassing event that is evidence for catastrophic disruption [*Keil et al.*, 1994; *Swindle et al.*, 2009].

[47] 2. A melt rock clast in the Plainview H chondrite breccia exhibits petrographic characteristics that suggest it cooled very slowly, possibly like the petrographically similar L chondrite impact melt rock Miller Range 05029. Both rocks have poikilitic textures of mm size low-Ca pyroxene and plagioclase that overgrew ~0.1 mm size olivine crystals. Moreover, they both display a strong depletion of metal and troilite, while plagioclase is strongly enriched [*Fodor and Keil*, 1976b; *Keil et al.*, 1980; J. R. Weirich et al., The Ar-Ar age and petrology of Miller Range 05029: An impact melt from the very early solar system, submitted to *Meteoritics and Planetary Science*, 2010]. Miller Range 05029 indicates metallographic cooling at ~14°C/Ma and likely formed at a large, shattering impact on the accreting L chondrite parent asteroid [*Wittmann et al.*, 2009; J. R. Weirich et al., submitted manuscript, 2010]. If a similar scenario is invoked for the Plainview clast, then a shattering and scrambling impact may have affected the H chondrite parent asteroid between ~3700 and 3630 Ma. This relationship was previously inferred by *Folco et al.* [2004] from their study of DaG 896 and by *Gaffey and Gilbert* [1998], who linked 4500 to 3700 Ma ages of IIE irons to impacts on the H chondrite asteroid. Three 0.5 to 1 cm size lithic fragments in the Abbott H chondrite regolith breccia are granular- to pokilitic-textured melt rocks that are depleted in opaque phases [*Fodor et al.*, 1976; *Rubin and Bottke*, 2009]. *Fodor et al.* [1976] remarked that these clasts are similar to the melt clasts in the Plainview meteorite. These clasts should record a formation before ~3600 Ma, if the inference is correct that no such melt rocks formed on what remained of the H chondrite parent asteroid after that time.

[48] 3. A lithic fragment in the H5 regolith breccia Eva has a metal- and troilite-depleted spinifex-like texture of ~0.2 mm size olivine phenocrysts in a glassy melt matrix. This clast was interpreted as an impact melt fragment of H chondrite parentage [*Fodor and Keil*, 1976a; *Ruzicka et al.*, 1998]. Although no age data are available for this clast, its petrographic characteristics are similar to melt clasts in DaG 896, Ourique, NWA 2457, Dhofar 323, and Yamato-79046, implying formation before 3600 Ma ago.

[49] 4. A probable solar system evolutionary context for the early major collisions that affected the H chondrite

Table A1. Proportion of Shock Melted Antarctic Meteorites Based On Records of the National Institute of Polar Research From 1996–2009[a]

Reference[b]	Total Mass[c] (g)	Number of Described H Chondrites	Partially Shock Melted[d]		Shock Melt Veins and Isolated Pockets[e]		All Associations With Shock Melts[f]	
			Grams	Percent	Grams	Percent	Grams	Percent
1	11129.0	105	20.2	0.2	190.2	1.9	210.4	1.9
2	26763.6	226	53.0	0.2	300.1	1.1	353.1	1.3
3	29469.4	114	167.8	0.6	39.2	0.1	207.0	0.7
4	24422.3	129	ND	NA	261.6	1.1	261.6	1.1
5	12399.2	132	ND	NA	ND	NA	ND	NA
6	10880.4	142	1223.8	11.3	82.0	0.8	1305.8	12.0
7	65820.8	389	19.9	NA	647.7	1.0	667.6	1.0
8	29498.0	85	ND	NA	ND	NA	ND	NA
9	3330.8	55	ND	NA	6.4	NA	6.4	NA
10	7625.9	167	65.0	0.9	16.5	0.2	81.5	1.1
1–10	221339.4	1544	1550	0.7	1544	0.7	3093	1.4

[a]NA, not applicable; ND, none described.
[b]1, *Kojima and Yanai* [1996]; 2, *Kojima and Imae* [1998]; 3, *Kojima and Imae* [2000]; 4, *Kojima* [2001]; 5, *Kojima and Imae* [2002]; 6, *Kojima and Imae* [2003]; 7, *Kojima and Yamaguchi* [2005]; 8, *Kojima and Yamaguchi* [2007]; 9, *Kojima and Yamaguchi* [2008]; 10, *Kojima et al.* [2009].
[c]Total mass of described H chondrites in the respective reference.
[d]Designated as "meteorite experienced partial melting, an glass due to the melting occurs locally but not as pockets" in references 1–6 and "melted" in references 7–10.
[e]Designated as "shock melt pocket is observed" in references 1–6, and "shock vein" in references 7–10.
[f]Sum data of partially shock melted and shock melt veins and isolated pockets.

Table A2. Electron Microprobe Analysis Data for Clast Olivine[a]

	Parameter	MgO (wt %)	SiO_2 (wt %)	CaO (wt %)	Cr_2O_3 (wt %)	FeO[b] (wt %)	MnO (wt %)	Total (wt %)	AFU[c]	Mg[d]	Fa[e]
LAP 04462 n = 74	minimum	41.80	38.62	ND	ND	13.59	0.36	98.50	2.98	80.58	14.45
	maximum	45.73	40.28	0.20	0.65	17.47	0.60	100.44	3.00	85.16	18.97
	mean	43.10	39.46	0.05	0.11	15.99	0.48	99.28	2.99	82.34	17.23
	σ	0.75	0.28	0.05	0.13	0.85	0.05	0.42	0.005	0.99	0.98
LAP 02240 n = 36	minimum	42.32	39.05	ND	ND	13.94	0.39	98.75	2.98	81.33	14.86
	maximum	44.79	40.58	0.08	0.09	16.88	0.56	99.98	3.00	84.75	18.20
	mean	43.10	39.76	0.03	0.02	15.75	0.49	99.26	2.99	82.55	17.01
	σ	0.43	0.30	0.02	0.03	0.56	0.05	0.29	0.005	0.62	0.62
LAP 03922 n = 25	minimum	42.53	39.04	ND	ND	15.15	0.42	99.05	2.98	81.63	16.16
	maximum	44.10	40.00	0.08	0.10	16.69	0.58	99.80	3.00	83.38	17.86
	mean	43.00	39.39	0.03	0.03	16.02	0.50	99.44	2.99	82.27	17.28
	σ	0.33	0.26	0.02	0.03	0.37	0.04	0.23	0.005	0.39	0.38
LAP 04751 n = 16	minimum	42.62	39.15	0.01	ND	15.69	0.39	99.02	2.99	81.89	16.93
	maximum	43.82	39.85	0.07	0.18	16.40	0.58	100.34	3.00	82.62	17.66
	mean	43.14	39.53	0.04	0.05	16.09	0.47	99.40	2.99	82.28	17.30
	σ	0.26	0.18	0.02	0.04	0.22	0.05	0.33	0.003	0.24	0.24
LAP 031125 n = 50	minimum	42.04	39.14	ND	ND	14.02	0.40	98.62	2.98	81.52	15.15
	maximum	44.21	40.48	0.14	0.42	16.59	0.57	100.18	3.00	84.42	18.02
	mean	43.34	39.80	0.06	0.12	15.53	0.49	99.43	2.99	82.82	16.74
	σ	0.51	0.22	0.04	0.11	0.56	0.04	0.35	0.003	0.64	0.64
LAP 031173 n = 27	minimum	42.53	39.13	0.01	ND	15.53	0.44	98.60	2.99	81.91	16.73
	maximum	43.44	39.77	0.14	0.09	16.36	0.56	99.75	3.00	82.81	17.64
	mean	43.00	39.47	0.05	0.03	15.98	0.50	99.14	2.99	82.29	17.26
	σ	0.24	0.17	0.03	0.02	0.22	0.04	0.34	0.003	0.23	0.23
LAP 031308 n = 54	minimum	41.53	39.3	ND	ND	15.43	0.39	98.52	2.98	80.61	17.20
	maximum	43.50	40.17	0.11	0.43	16.87	0.59	99.74	3.00	82.34	18.90
	mean	42.68	39.68	0.04	0.05	15.99	0.49	99.07	2.99	81.85	17.71
	σ	0.30	0.18	0.02	0.07	0.27	0.04	0.31	0.004	0.30	0.30

[a]ND, none detected; typically, Al_2O_3, Na_2O, P_2O_5, K_2O, TiO_2, NiO were near or below detection.
[b]All Fe as FeO.
[c]Atomic formula unit based on four oxygen atoms.
[d]Mg number as mole ratios of 100 × [Mg/(Mg + Fe + Mn)].
[e]Values are mole ratios.

Table A3. Electron Microprobe Analysis Data for Clast Low-Ca Pyroxene[a]

	Parameter	MgO (wt %)	Al_2O_3 (wt %)	SiO_2 (wt %)	CaO (wt %)	TiO_2 (wt %)	Cr_2O_3 (wt %)	FeO[b] (wt %)	MnO (wt %)	Total (wt %)	AFU[c]	Mg[d,e]	En[e]	Fs[e]	Wo[e]
LAP 04462 n = 60	minimum	30.62	0.08	55.72	0.18	0.03	0.10	7.99	0.39	98.81	3.99	82.36	82.07	11.93	0.35
	maximum	33.59	0.53	57.41	1.75	0.26	1.09	11.34	0.61	100.30	4.01	87.31	87.42	16.83	3.43
	mean	31.60	0.22	56.43	0.80	0.16	0.29	9.50	0.51	99.55	4.00	84.91	84.25	14.21	1.54
	σ	0.58	0.08	0.37	0.27	0.05	0.19	0.70	0.05	0.36	0.006	1.09	1.21	1.06	0.52
LAP 02240 n = 37	minimum	30.62	0.06	55.86	0.47	0.01	0.06	8.82	0.41	98.97	3.98	83.01	82.72	13.45	0.92
	maximum	31.67	1.10	57.01	1.66	0.61	0.78	10.90	0.60	100.53	4.01	85.51	84.93	16.22	3.22
	mean	31.19	0.40	56.60	0.71	0.18	0.31	9.84	0.51	99.80	3.99	84.30	83.79	14.83	1.38
	σ	0.25	0.30	0.35	0.22	0.13	0.22	0.38	0.04	0.38	0.005	0.50	0.53	0.51	0.44
LAP 03922 n = 34	minimum	30.28	0.03	55.57	0.51	ND	0.06	9.49	0.41	98.61	3.98	82.18	81.43	14.40	0.96
	maximum	31.64	0.48	57.07	0.88	0.28	0.60	11.20	0.64	100.63	4.01	84.81	84.38	16.90	1.69
	mean	31.22	0.17	56.46	0.66	0.12	0.14	10.12	0.52	99.51	4.00	83.93	83.54	15.20	1.27
	σ	0.27	0.11	0.38	0.09	0.06	0.10	0.28	0.05	0.42	0.006	0.41	0.47	0.39	0.18
LAP 04751 n = 42	minimum	29.71	0.05	55.73	0.26	ND	0.08	9.39	0.42	99.08	3.98	81.61	80.81	14.17	0.50
	maximum	31.78	2.01	57.14	1.36	0.39	0.39	11.68	0.62	100.51	4.01	84.93	84.71	17.57	2.62
	mean	31.20	0.27	56.49	0.67	0.14	0.15	10.04	0.52	99.60	4.00	84.03	83.62	15.10	1.28
	σ	0.41	0.32	0.35	0.17	0.09	0.07	0.39	0.05	0.37	0.006	0.60	0.70	0.59	0.34
LAP 031125 n = 72	minimum	30.54	0.06	55.77	0.34	0.02	0.03	7.55	0.31	99.08	3.98	82.97	82.48	11.19	0.66
	maximum	33.06	0.92	57.50	1.30	0.46	0.95	10.93	0.62	100.59	4.01	88.20	87.48	16.18	2.53
	mean	31.44	0.27	56.77	0.73	0.16	0.29	9.68	0.49	99.90	3.99	84.63	84.08	14.52	1.40
	σ	0.47	0.18	0.39	0.17	0.10	0.20	0.56	0.05	0.31	0.005	0.90	0.96	0.86	0.33
LAP 031173 n = 18	minimum	30.39	0.12	55.65	0.34	0.08	0.06	9.82	0.45	98.59	3.99	82.59	81.74	14.81	0.66
	maximum	31.99	0.68	57.08	0.93	0.21	0.67	10.91	0.57	100.50	4.01	84.36	84.35	16.47	1.78
	mean	31.24	0.20	56.35	0.69	0.14	0.16	10.12	0.52	99.49	4.00	83.95	83.51	15.18	1.31
	σ	0.34	0.13	0.36	0.12	0.03	0.13	0.26	0.03	0.49	0.005	0.41	0.53	0.39	0.24
LAP 031308 n = 47	minimum	30.41	0.03	55.95	0.49	0.01	0.01	9.52	0.44	98.88	3.98	83.05	82.49	14.76	0.91
	maximum	31.71	0.64	57.23	1.19	0.25	0.79	10.51	0.60	100.31	4.00	84.31	83.83	16.03	2.30
	mean	31.10	0.20	56.70	0.69	0.12	0.15	10.00	0.52	99.58	3.99	83.75	83.30	15.38	1.32
	σ	0.28	0.13	0.30	0.15	0.06	0.12	0.20	0.04	0.35	0.004	0.27	0.31	0.27	0.29

[a]ND, none detected; typically, Na_2O, P_2O_5, K_2O, and NiO were near or below detection.
[b]All Fe as FeO.
[c]Atomic formula unit based on six oxygen atoms.
[d]Mg number as mole ratios of 100 × [Mg/(Mg + Fe + Mn)].
[e]Values are mole ratios.

Table A4. Electron Microprobe Analysis Data for Clast High-Ca Pyroxene[a]

	Na_2O (wt %)	P_2O_5 (wt %)	MgO (wt %)	Al_2O_3 (wt %)	SiO_2 (wt %)	K_2O (wt %)	CaO (wt %)	TiO_2 (wt %)	NiO (wt %)	Cr_2O_3 (wt %)	FeO[b] (wt %)	MnO (wt %)	Total (wt %)	AFU[c]	Mg[d,e]	En[e]	Fs[e]	Wo[e]
LAP 03922 augite	0.66	0.19	19.66	1.87	55.74	0.1	16.21	0.27	0.03	0.48	5.47	0.36	101.06	3.98	85.71	57.17	8.93	33.90
LAP 031173 diopside	0.57	0.22	16.91	0.93	53.59	0.01	22.75	0.44	0.06	0.93	3.29	0.30	99.98	4.01	89.42	48.19	5.23	46.57
	0.50	0.28	17.13	0.50	53.94	0.01	22.81	0.43	0.00	0.75	3.25	0.29	99.90	4.00	89.62	48.47	5.15	46.39
	0.55	0.25	17.39	0.65	54.31	0.02	22.80	0.40	0.06	0.75	3.23	0.24	100.65	4.01	89.94	48.86	5.10	46.05
LAP 031308 augite	0.47	0.22	18.66	0.54	54.55	ND	20	0.44	0.03	0.69	3.79	0.31	99.69	3.99	88.84	53.02	6.19	40.80
LAP 031308 diopside	0.6	0.25	16.91	0.53	54.66	0.01	23.18	0.4	0.04	0.74	2.93	0.23	100.48	4.00	90.31	47.95	4.78	47.27
	0.56	0.28	17.08	0.51	54.14	0.01	23.04	0.4	ND	1.22	3.67	0.21	101.14	4.01	88.39	47.77	5.91	46.32
	0.53	0.25	17.25	0.52	54.34	ND	23.39	0.45	0.05	0.73	3.24	0.2	100.96	4.01	89.77	48.04	5.17	46.80
	0.57	0.22	17.61	0.44	54.01	ND	22.4	0.14	ND	0.86	3.5	0.22	99.96	4.01	89.12	49.31	5.66	45.03
	0.58	0.24	17.18	0.48	54.31	ND	23.25	0.17	0.02	0.89	3.43	0.19	100.75	4.01	89.16	47.91	5.52	46.57
LAP 04751 pigeonite	0.05	0.05	29.77	0.11	56.49	0.00	2.91	0.08	0.08	0.18	9.23	0.38	99.33	3.99	84.66	80.4	14.0	5.7
	2.27	0.18	22.91	5.22	56.16	0.18	3.50	0.11	0.16	0.25	9.34	0.33	100.62	3.99	80.83	74.7	17.1	8.2
	0.10	0.12	27.48	0.15	56.02	0.01	5.95	0.11	0.01	0.31	8.64	0.39	99.29	3.99	84.41	75.1	13.2	11.7
	0.23	0.11	27.09	0.23	56.28	0.01	7.25	0.12	0	0.31	7.89	0.55	100.07	4.00	85.11	73.8	12.1	14.2
	0.29	0.06	24.26	1.11	54.31	0.04	8.73	0.11	0.13	0.34	9.92	0.42	99.73	4.01	80.71	67.2	15.4	17.4
LAP 04751 augite	0.36	0.13	24.87	0.25	54.93	0.00	10.65	0.13	0.05	0.41	7.03	0.38	99.17	4.01	85.68	68.20	10.81	20.99
	1.30	0.20	21.05	2.97	55.56	0.12	12.98	0.13	0.06	0.60	5.16	0.32	100.45	3.99	87.26	63.27	8.69	28.04
	0.35	0.19	21.85	0.52	55.03	0.02	15.10	0.20	0.00	0.49	5.27	0.38	99.39	3.99	87.31	61.27	8.29	30.44
	0.42	0.23	21.65	0.33	54.90	0.02	16.21	0.08	0.00	0.69	4.28	0.39	99.20	4.00	89.18	60.63	6.74	32.64
	0.53	0.20	19.02	0.29	55.06	0.00	18.50	0.12	0.03	1.19	4.79	0.25	99.98	3.99	87.06	54.35	7.67	37.98
	0.62	0.21	17.97	1.00	55.23	0.05	20.43	0.32	0.00	0.64	3.63	0.28	100.39	3.98	89.09	51.80	5.88	42.33
	0.52	0.30	17.56	0.68	53.99	0.01	20.76	0.08	0.10	0.70	4.15	0.27	99.12	4.00	87.64	50.45	6.68	42.87
	4.06	0.20	13.67	3.88	56.30	0.32	16.97	0.24	0.02	0.69	2.65	0.24	99.26	4.01	89.40	49.97	5.43	44.59
LAP 04751 diopside	0.48	0.25	17.20	0.36	54.45	0.00	21.86	0.31	0.00	0.79	3.34	0.24	99.29	3.99	89.54	49.44	5.38	45.18
	1.08	0.27	16.40	1.25	54.57	0.09	21.26	0.21	0.02	0.66	3.58	0.24	99.61	4.00	88.46	48.69	5.95	45.36
	0.54	0.25	17.24	0.34	54.22	0.03	22.33	0.27	0.04	0.87	3.45	0.28	99.86	4.00	89.17	48.95	5.49	45.56
	0.50	0.30	17.27	0.29	54.95	0.00	22.31	0.10	0.02	0.99	3.24	0.25	100.23	3.99	89.83	49.18	5.17	45.65

[a]ND, none detected.
[b]All Fe as FeO.
[c]Atomic formula unit based on six oxygen atoms.
[d]Mg number as mole ratios of 100 × [Mg/(Mg + Fe + Mn)].
[e]Values are mole ratios.

Table A5. Electron Microprobe Analysis Data for Clast Mesostases and Feldspar[a]

	Na_2O (wt %)	P_2O_5 (wt %)	MgO (wt %)	Al_2O_3 (wt %)	SiO_2 (wt %)	K_2O (wt %)	CaO (wt %)	TiO_2 (wt %)	NiO (wt %)	Cr_2O_3 (wt %)	FeO (wt %)	MnO (wt %)	Total (wt %)	Total AFU[b]	Na[c]	Ca[c]	K[c]
LAP 04462	4.14	0.07	1.13	19.37	60.58	0.69	3.41	0.39	0.79	0.12	9.84	0.03	100.55	4.89	35.46	15.82	4.88
LAP 03922	8.13	0.05	0.18	21.81	63.13	0.15	2.94	0.02	0.65	ND	1.73	0.02	98.8	4.95	82.50	16.45	1.05
	3.44	0.1	0.37	20.18	71.53	0.8	2.82	0.14	0.01	ND	1.46	0.06	100.91	4.60	62.28	28.07	9.65
	6.95	0.1	0.76	22.51	62.67	0.2	5.47	0.15	0.25	0.02	2.07	0.01	101.16	4.94	68.75	29.86	1.39
	7.8	0.07	3.29	19.13	62.97	0.16	3.69	0.07	0.13	0.03	1.68	ND	99.01	5.00	78.41	20.55	1.04
LAP 04751	**9.56**	**0.05**	**0.26**	**21.34**	**64.28**	**0.97**	**2.41**	**0.05**	**0.03**	**0.03**	**0.73**	**0.01**	**99.74**	**5.02**	**82.90**	**11.57**	**5.53**
	9.67	**0.06**	**0.03**	**21.47**	**65.05**	**0.91**	**2.41**	**0.07**	**0.10**	**0.01**	**0.78**	**ND**	**100.55**	**5.01**	**83.32**	**11.50**	**5.18**
	8.79	0.06	1.89	19.95	64.26	0.35	4.43	0.13	0.01	0.06	0.77	0.03	100.71	5.02	76.64	21.36	2.00
LAP 031125	0.39	0.06	0.17	18.87	75.86	0.83	1.01	0.38	0.1	ND	1.13	0.04	98.82	4.34	25.82	37.50	36.68
	4.04	0.03	0.19	18.82	74.27	1.02	1.1	0.46	0.08	0.02	1.31	0.04	101.39	4.58	75.94	11.42	12.64
	3.22	0.09	1.7	15.86	74.57	1.03	0.81	0.31	ND	0.01	1.13	0.07	98.79	4.54	74.15	10.21	15.64
	4.19	0.2	0.3	18.03	75.52	1.08	0.9	0.46	0.05	0.02	0.81	0.04	101.61[d]	4.57	77.66	9.19	13.15
	4.52	0.06	0.21	19.97	72.83	1.05	1.51	0.67	0.01	0.04	0.83	0.04	101.74[d]	4.62	74.81	13.77	11.41
LAP 031173	8.65	0.07	0.38	20.59	61.55	0.42	3.42	0.05	1.23	0.02	3.85	ND	100.22	5.05	79.98	17.49	2.53
	9.29	0.06	0.38	21.27	63.63	0.62	2.56	ND	0.51	0.01	2.01	0.03	100.35	5.03	83.61	12.73	3.65
	4.05	0.25	1.48	17.79	66.51	0.78	5.54	0.18	0.04	0.03	2.4	0.07	99.1	4.75	53.12	40.18	6.70
LAP 031308	**9.72**	**0.05**	**0.02**	**22.11**	**65.09**	**0.47**	**3.11**	**0.06**	**0.02**	**0.18**	**0.51**	**ND**	**101.34**	**5.01**	**82.71**	**14.67**	**2.61**
	9.77	**ND**	**0.01**	**21.93**	**65.66**	**1.01**	**2.46**	**0.05**	**ND**	**0.02**	**0.42**	**0.04**	**101.37**	**5.01**	**82.85**	**11.53**	**5.62**
	9.76	**0.02**	**0.07**	**22.34**	**64.42**	**0.59**	**2.69**	**0.06**	**0.01**	**0.05**	**0.83**	**0.06**	**100.9**	**5.02**	**83.85**	**12.82**	**3.33**
	9.96	**0.02**	**0.26**	**22.49**	**64.95**	**0.27**	**2.68**	**0.03**	**ND**	**0.01**	**0.75**	**0.02**	**101.44**	**5.02**	**85.74**	**12.73**	**1.53**
	10.08	0.05	0.03	21.25	65.65	0.96	2.24	0.02	0.09	ND	0.67	0.04	101.07	5.03	84.35	10.33	5.31
	9.48	0.01	1.39	19.71	65.79	0.61	3.27	0.04	ND	0.02	0.56	0.02	100.89	5.02	81.11	15.48	3.42
	10.27	0.02	0.64	20.79	66.4	0.39	2.16	0.06	ND	ND	0.75	0.01	101.5	5.02	87.58	10.20	2.22
	3.4	0.32	2.96	18.63	68.25	0.78	3.35	0.16	0.03	0.11	2.37	0.15	100.52	4.70	58.97	32.16	8.87
	3.4	0.11	1.02	21.06	70.25	0.85	2.44	0.13	0.04	0.05	1.46	0.1	100.92	4.63	64.01	25.51	10.48
	3.74	0.07	1.32	19.85	71.55	0.93	2.24	0.11	0.07	0.04	1.2	0.04	101.16	4.63	66.96	22.17	10.87
	8.39	0.05	5.26	16.1	59.77	0.83	6.18	0.1	0.05	0.76	1.07	0.06	98.63	5.18	67.96	27.60	4.43
	9.94	0.06	0.03	22.29	63.66	0.37	2.77	0.07	0.13	0.02	1.9	0.07	101.32	5.05	84.82	13.09	2.10

[a]ND none detected; no reliable analyses were produced from thin section LAP 02240; all Fe as FeO; stoichiometric feldspar analyses are printed in bold.
[b]Atomic formula units, based on eight oxygen atoms.
[c]Mole ratio calculated from $100 \times [Na/(Na^+Ca + K)]$, $100 \times [Ca/(Na^+Ca + K)]$, and $100 \times [K/(Na^+Ca + K)]$, respectively.
[d]Note poor totals.

Table A6. Electron Microprobe Analysis Data for Melt Matrix Olivine[a]

	Parameter	MgO (wt %)	Al_2O_3 (wt %)	SiO_2 (wt %)	CaO (wt %)	Cr_2O_3 (wt %)	FeO[b] (wt %)	MnO (wt %)	Total (wt %)	AFU[c]	Mg[d]	Fa[e]
LAP 04462 n = 4	minimum	42.52	0.02	38.90	0.03	0.33	13.77	0.39	99.06	2.98	82.10	14.75
	maximum	44.70	0.38	40.32	0.25	0.68	15.97	0.55	100.20	3.00	84.90	17.40
	mean	43.70	0.18	39.64	0.16	0.53	14.93	0.47	99.65	2.99	83.49	16.10
	σ	0.92	0.18	0.65	0.09	0.16	1.11	0.08	0.48	0.007	1.33	1.25
LAP 02240 n = 21	minimum	42.67	ND	39.39	0.02	ND	13.39	0.42	98.55	2.98	82.62	14.28
	maximum	45.09	0.31	40.11	0.24	0.58	15.52	0.56	99.57	2.99	85.20	16.91
	mean	43.52	0.07	39.70	0.10	0.24	14.73	0.49	98.99	2.99	83.59	15.96
	σ	0.55	0.07	0.20	0.06	0.13	0.59	0.04	0.28	0.004	0.66	0.68
LAP 03922 n = 7	minimum	42.29	ND	38.88	0.02	0.01	12.47	0.31	99.05	2.99	81.53	13.30
	maximum	45.64	0.21	40.00	0.25	0.89	16.58	0.59	99.80	3.01	86.39	18.02
	mean	43.64	0.09	39.50	0.10	0.31	15.17	0.46	99.44	3.00	83.25	16.33
	σ	1.23	0.09	0.44	0.09	0.33	1.72	0.10	0.23	0.005	1.98	1.91
LAP 04751 n = 6	minimum	41.88	ND	39.24	0.07	0.03	15.29	0.39	99.40	2.97	81.22	16.85
	maximum	43.24	0.28	40.34	0.28	0.62	17.15	0.49	99.89	3.00	82.77	18.42
	mean	42.70	0.08	40.00	0.13	0.18	15.88	0.45	99.58	2.98	82.34	17.25
	σ	0.48	0.11	0.39	0.08	0.23	0.65	0.04	0.19	0.010	0.57	0.59
LAP 031125 n = 6	minimum	41.96	0.02	39.61	0.03	0.30	15.07	0.44	98.74	2.98	81.92	16.20
	maximum	43.68	0.12	39.95	0.24	0.62	16.05	0.54	99.77	2.99	83.33	17.66
	mean	42.77	0.06	39.77	0.16	0.45	15.60	0.49	99.37	2.98	82.56	16.98
	σ	0.62	0.04	0.12	0.07	0.12	0.40	0.04	0.39	0.003	0.55	0.55
LAP 031173 n = 5	minimum	42.66	ND	39.51	0.07	0.06	14.80	0.44	99.22	2.99	81.91	15.66
	maximum	44.65	0.40	40.00	0.28	0.19	16.47	0.53	100.37	3.00	83.96	17.67
	mean	43.30	0.12	39.68	0.12	0.10	15.74	0.47	99.61	2.99	82.64	16.94
	σ	0.79	0.17	0.19	0.09	0.06	0.61	0.03	0.48	0.004	0.78	0.76
LAP 031308 n = 8	minimum	42.21	0.02	39.30	0.02	0.02	14.75	0.45	98.66	2.98	81.11	16.43
	maximum	43.45	0.09	40.48	0.16	0.19	16.69	0.54	99.68	3.00	83.10	18.48
	mean	42.84	0.04	39.81	0.08	0.08	15.74	0.48	99.18	2.99	82.13	17.43
	σ	0.43	0.03	0.36	0.04	0.05	0.68	0.03	0.32	0.007	0.71	0.72

[a]ND, none detected; typically, Na_2O, P_2O_5, K_2O, TiO_2, NiO were near or below detection.
[b]All Fe as FeO.
[c]Atomic formula unit based on four oxygen atoms.
[d]Mg number as mole ratios of 100 × [Mg/(Mg + Fe + Mn)].
[e]Values are mole ratios.

Table A7. Electron Microprobe Analysis Data for Melt Matrix Low-Ca Pyroxene[a]

	Parameter	MgO (wt %)	Al_2O_3 (wt %)	SiO_2 (wt %)	CaO (wt %)	TiO_2 (wt %)	Cr_2O_3 (wt %)	FeO[b] (wt %)	MnO (wt %)	Total (wt %)	AFU[c]	Mg[d]	En[e]	Fs[e]	Wo[e]
LAP 04462 n = 6	minimum	31.22	0.19	55.87	0.68	0.04	0.13	7.93	0.36	99.47	3.99	83.95	83.49	11.80	1.30
	maximum	32.69	0.48	57.11	1.29	0.21	1.26	10.30	0.51	100.59	4.01	87.47	86.71	15.21	2.52
	mean	31.83	0.29	56.46	0.90	0.10	0.80	9.07	0.44	99.97	4.00	85.65	84.74	13.53	1.73
	σ	0.49	0.11	0.47	0.26	0.07	0.47	0.85	0.05	0.39	0.009	1.26	1.19	1.21	0.51
LAP 02240 n = 19	minimum	30.68	0.13	55.52	0.23	0.06	0.11	7.12	0.29	98.60	3.98	83.90	82.79	10.87	0.43
	maximum	33.08	0.67	57.38	1.07	0.32	1.09	10.09	0.59	100.28	4.00	88.47	87.04	15.28	2.08
	mean	31.45	0.28	56.60	0.69	0.16	0.31	9.35	0.49	99.38	3.99	85.05	84.56	14.11	1.33
	σ	0.59	0.14	0.43	0.22	0.08	0.23	0.71	0.07	0.41	0.006	1.12	1.17	1.07	0.43
LAP 03922	1	31.25	0.26	55.76	0.66	0.23	0.37	10.51	0.5	99.66	4.01	83.50	83.08	15.66	1.26
	2	31.55	0.11	56.48	0.64	0.11	0.08	10.06	0.55	99.6	4.00	84.13	83.79	15.00	1.21
LAP 04751 n = 4	minimum	31.36	0.11	56.61	0.61	0.03	0.11	9.09	0.49	99.75	3.99	83.68	83.25	13.62	1.17
	maximum	31.8	0.35	57.49	0.7	0.34	0.28	10.43	0.52	100.84	4.00	85.57	85.05	15.48	1.33
	mean	31.51	0.23	56.98	0.66	0.16	0.19	9.98	0.50	100.27	3.99	84.30	83.88	14.87	1.25
	σ	0.20	0.10	0.39	0.04	0.14	0.08	0.63	0.02	0.56	0.004	0.89	0.84	0.88	0.07
LAP 031125 n = 5	minimum	31.50	0.14	57.25	0.54	0.02	0.19	7.70	0.37	100.04	3.98	84.46	84.07	11.46	1.02
	maximum	32.77	0.22	57.60	0.72	0.20	0.84	9.83	0.56	100.62	4.00	87.88	87.15	14.70	1.39
	mean	32.23	0.18	57.47	0.66	0.09	0.50	8.72	0.44	100.37	3.99	86.24	85.74	13.01	1.25
	σ	0.54	0.03	0.14	0.07	0.07	0.30	0.92	0.08	0.25	0.004	1.48	1.30	1.38	0.15
LAP 031173 n = 4	minimum	30.36	0.02	56.44	0.64	0.01	0.10	9.78	0.43	99.38	3.99	83.75	82.28	14.58	1.21
	maximum	31.57	0.61	56.49	1.35	0.23	0.39	9.99	0.62	100.09	4.00	84.51	83.95	15.08	2.63
	mean	31.23	0.27	56.47	0.85	0.12	0.20	9.92	0.54	99.69	4.00	84.18	83.49	14.86	1.65
	σ	0.58	0.25	0.02	0.34	0.09	0.13	0.10	0.08	0.30	0.005	0.34	0.81	0.21	0.67
LAP 031308 n = 8	minimum	29.83	0.13	56.46	0.64	0.08	0.10	9.54	0.46	99.85	3.99	82.12	81.23	14.92	1.23
	maximum	31.31	0.74	57.16	1.93	0.27	0.67	10.99	0.58	100.22	4.00	83.81	83.22	16.97	3.80
	mean	30.67	0.40	56.69	0.96	0.15	0.30	10.22	0.51	99.99	3.99	83.28	82.38	15.77	1.86
	σ	0.49	0.24	0.23	0.43	0.06	0.20	0.43	0.05	0.14	0.006	0.53	0.78	0.60	0.85

[a]Typically, Na_2O, P_2O_5, K_2O, and NiO were near or below detection.
[b]All Fe as FeO.
[c]Atomic formula unit based on six oxygen atoms.
[d]Mg number as mole ratios of 100 × [Mg/(Mg + Fe + Mn)].
[e]Values are mole ratios.

asteroid is the epoch of collisional growth of protoplanets and the mutual perturbations of planetary embryos after runaway accretion cleared dispersed dust [*Bottke et al.*, 2005]. This epoch lasted until ~100 Ma after formation of CAI [*Weidenschilling and Cuzzi*, 2006], which means that such collisions would have affected the H chondrite parent asteroid during cooling from metamorphism. The Portales Valley meteorite [*Bogard and Garrison*, 2009], and melt rock clasts in Dhofar 323 [*Korochantseva et al.*, 2008], NWA 2457 [*Fernandes et al.*, 2006], and possibly Ourique [*Swindle et al.*, 2009] are evidence for this early bombardment.

Appendix A

A1. Appraisal of Impact-Melted H Chondrite Meteorites

[50] *Keil et al.* [1997] estimated that only <0.001 vol % of impact-generated debris would be melted over the typical lifetime of an asteroid, yet the proportion of melt being found by meteorite recovery programs is much larger. Since 1996, the National Institute of Polar Research in Tokyo noted shock petrographic observations in their classification of meteorites from Asuka Station and the Yamato Mountains in Antarctica. Of these, 1318 with a total mass of 194.58 kg are H chondrites and about 0.7% of this mass is described as shock melted and another ~0.7% contains shock melt veins (Table A1). These values are 2–3 orders of magnitude greater than that anticipated. Furthermore, additional melt volumes lurk as incompletely classified specimens. *Niihara et al.* [2007], for example, described the 2.14 kg Yamato-791088 H-chondrite as a clast-rich impact melt rock, but it is officially classified as a H6. This example implies a far larger fraction of H chondrites may be impact melts. Thus, it is safe to anticipate the collection of impact melt will continue to grow. Electron microprobe analysis (EMPA) data for lithic clast components entrained in the impact melts that were the subjects of this study are listed in Tables A2–A5 and EMPA data for mineral phases crystallized from these impact melts are presented in Tables A6 and A7.

A2. Stage 2 Cooling Rate Calculation for Rose City

[51] Because the phase diagram for Fe-Ni with P saturation [*Yang et al.*, 1996] and the Ni-Fe diffusion coefficient were revised since the work of *Smith and Goldstein* [1977], the stage 2 metallographic cooling rate for Rose City was recalculated according to the method of *Taylor et al.* [1979]. Assuming isothermal growth of kamacite, a cooling rate was calculated from the average width of secondary kamacite (20 μm thickness) and the bulk concentration of Ni in metal particles of Rose City (9 wt %) reported by *Smith and Goldstein* [1977]. By using the Ni diffusion coefficient of *Hopfe and Goldstein* [2001]:

$$D^{\gamma}_{ternary} = 10 \times \exp(1.188 + 0.0185 \times C_{Ni}) \times \exp\left[(-76668 - 116.112 \times C_{Ni}) \times (RT)^{-1}\right],$$

with the concentration of Ni (C_{Ni}), gas constant (R), and the temperature (T), an equivalent time needed for growing the observed amount of kamacite by diffusion is 1.18×10^{10} s (~376 years), the temperature for optimum growth is 688°C and beginning of nucleation is at 740°C. This would translate to a cooling rate in that temperature interval of 0.14°C/a. However, following *Taylor et al.* [1979], the Ni concentration of 6.1 ± 0.2 wt % kamacite in metal particles of Rose City [*Smith and Goldstein*, 1977] indicates a temperature for final equilibration at 604°C in the Ni-Fe-P phase diagram of *Yang et al.* [1996]. This suggests kamacite growth over the temperature interval between 740 and 604°C and a cooling rate of 0.36°C/a (1.2×10^{-8} °C/s). This recalculated time of optimum growth is a little lower than the approximate cooling rate of ~1°C/a determined by *Smith and Goldstein* [1977], but well within the approximate error of 1 order of magnitude previously estimated for this method [*Taylor et al.*, 1979].

[53] In order to constrain the minimum stage 2 cooling rate of the seven LAP samples, a 1 μm thick kamacite rim can be assumed, which would have been at the detection limit of the electron microprobe procedure. For this calculation, the highest average Ni concentration in martensite of 9.54 wt % from all samples analyzed (Table 3) yields the longest equivalent time of growth of 3.0×10^8 s over the temperature interval between 672 and 721°C. This translates to a cooling rate of ~5°C/a ($\sim 1.6 \times 10^{-7}$ °C/s), which corresponds to an approximate burial shallower than ~100 m [*Smith and Goldstein*, 1977; *Taylor and Heymann*, 1971].

[54] **Acknowledgments.** We appreciate constructive reviews by D. Mittlefehldt, W. Bottke, and C. Corrigan and the editorial handling by R. Carlson and J. Plescia. The LaPaz Ice field samples investigated in this study were recovered by the Antarctic Search for Meteorites Program (ANSMET), which is funded and supported by NSF, NASA, and the Smithsonian Institution. Thin sections were provided by C. Satterwhite, K. Righter, and R. Harrington of the Astromaterials Curation Facility at NASA Johnson Space Center in Houston. A. Peslier, J. Herrin, and G. A. Robinson assisted with microprobe procedures at the Johnson Space Center Electron-Beam Facility. E. Scott pointed out latest work on the evolution of the H chondrite asteroid. This study was funded by NASA cosmochemistry grants NNX07AG55G (DAK) and NNX08AG59G (TDS). LPI contribution 1531.

References

Akridge, G., P. H. Benoit, and D. W. Sears (1998), Regolith and megaregolith formation of H chondrites: Thermal constraints on the parent body, *Icarus*, *132*, 185–195, doi:10.1006/icar.1998.5904.

Bennett, M. E., III, and H. Y. McSween (1996), Revised model calculations for the thermal histories of ordinary chondrite parent bodies, *Meteorit. Planet. Sci.*, *31*, 783–792.

Benoit, P. H., and D. W. G. Sears (1992), The breakup of a meteorite parent body and the delivery of meteorites to Earth, *Science*, *255*, 1685–1687, doi:10.1126/science.255.5052.1685.

Bogard, D. D. (1995), Impact ages of meteorites: A synthesis, *Meteorit. Planet. Sci.*, *30*, 244–268.

Bogard, D. D., and D. H. Garrison (2009), Ar–Ar and I–Xe ages and thermal histories of three unusual metal-rich meteorites, *Geochim. Cosmochim. Acta*, *73*, 6965–6983, doi:10.1016/j.gca.2009.08.009.

Bogard, D. D., L. Husain, and R. J. Wright (1976), ^{39}Ar-^{40}Ar dating of collisional events in chondrite parent bodies, *J. Geophys. Res.*, *81*, 5664–5678, doi:10.1029/JB081i032p05664.

Bottke, W. F. J., D. D. Durda, D. Nesvorný, R. Jedicke, A. Morbidelli, D. Vokrouhlicky, and H. Levison (2005), The fossilized size distribution of the main asteroid belt, *Icarus*, *175*, 111–140, doi:10.1016/j.icarus.2004.10.026.

Brearley, A. J., and R. H. Jones (1998), Chondritic meteorites, in *Planetary Materials*, edited by J. J. Papike, chap. 3, pp. 3.1–3.398, Mineral. Soc. of Am., Washington, D. C.

Britt, D. T., and C. M. Pieters (1994), Darkening in black and gas-rich ordinary chondrites: The spectral effects of opaque morphology and distribution, *Geochim. Cosmochim. Acta*, *58*, 3905–3919, doi:10.1016/0016-7037(94)90370-0.

Burbine, T. H., T. J. McCoy, A. Meibom, B. Gladman, and K. Keil (2002), Meteoritic parent bodies: Their number and identification, in *Asteroids III*, edited by W. F. Bottke Jr. et al., pp. 653–667, Univ. of Ariz. Press, Tucson.

Cheek, L. C., and D. A. Kring (2008), Cooling rate determination for H chondrite impact melt breccia LAP 02240, *Lunar Planet. Sci.*, *XXXIX*, Abstract 1169.

Connolly, H. C., C. Smith, G. Benedix, L. Folco, K. Righter, J. Zipfel, A. Yamaguchi, and H. C. Aoudjehane (2007a), The Meteoritical Bulletin, No. 92, 2007 September, *Meteorit. Planet. Sci.*, *42*, 1647–1694, doi:10.1111/j.1945-5100.2007.tb00596.x.

Connolly, H. C., J. Zipfel, L. Folco, C. Smith, R. Jones, G. Benedix, K. Righter, A. Yamaguchi, H. C. Aoudjehane, and J. N. Grossman (2007b), The Meteoritical Bulletin, No. 91, 2007 March, *Meteorit. Planet. Sci.*, *42*, 413–466, doi:10.1111/j.1945-5100.2007.tb00242.x.

Dressler, B. O., and W. U. Reimold (2001), Terrestrial impact melt rocks and glasses, *Earth Sci. Rev.*, *56*, 205–284, doi:10.1016/S0012-8252(01)00064-2.

Dressler, B. O., and W. U. Reimold (2004), Order or chaos? Origin and mode of emplacement of breccias in floors of large impact structures, *Earth Sci. Rev.*, *67*, 1–54, doi:10.1016/j.earscirev.2004.01.007.

Farley, K. A., D. Vokrouhlický, W. F. Bottke, and D. Nesvorný (2006), A late Miocene dust shower from the break-up of an asteroid in the main belt, *Nature*, *439*, 295–297, doi:10.1038/nature04391.

Fernandes, V. A., R. Burgess, A. Bischoff, and K. Metzler (2006), Ar composition of the melt lithology within the NWA 2457 breccia, paper presented at Meteoritical Society 69th Annual Meeting, abstract 5308, Lunar Planet. Inst., Houston, Tex.

Fodor, R. V., and K. Keil (1976a), A komatiite-like lithic fragment with spinifex texture in the Eva meteorite: Origin from a supercooled impact-melt of chondritic parentage, *Earth Planet. Sci. Lett.*, *29*, 1–6, doi:10.1016/0012-821X(76)90020-0.

Fodor, R. V., and K. Keil (1976b), Carbonaceous and non-carbonaceous lithic fragments in the Plainview, Texas, chondrite: Origin and history, *Geochim. Cosmochim. Acta*, *40*, 177–189, doi:10.1016/0016-7037(76)90175-7.

Fodor, R. V., K. Keil, L. L. Wilkening, D. D. Bogard, and E. K. Gibson (1976), Origin and history of a meteorite parent-body regolith breccia: Carbonaceous lithic fragments in the Abbott, New Mexico chondrite, *Spec. Publ. N. M. Geol. Soc.*, *6*, 206–218.

Fodor, R. V., K. Keil, M. Prinz, M.-S. Ma, A. V. Murali, and R. A. Schmitt (1980), Clast-laden melt-rock fragment in the Adams County, Colorado, H5 chondrite, *Meteoritics*, *15*, 41–62.

Folco, L., P. A. Bland, M. D'Orazio, I. A. Franchi, S. P. Kelley, and S. Rocchi (2004), Extensive impact melting on the H chondrite parent asteroid during the cataclysmic bombardment of the early solar system: Evidence from the achondritic meteorite Dar al Gani 896, *Geochim. Cosmochim. Acta*, *68*, 2379–2397, doi:10.1016/j.gca.2003.11.023.

Frank, E. A., A. Wittmann, and D. A. Kring (2009), Petrography and metallographic cooling rate of H chondrite impact melt breccia LAP 04751, *Lunar Planet. Sci.*, *XL*, Abstract 2034.

Fujimaki, H., K. Ishikawa, and K. Aoki (1994), Rb-Sr-isotopic study of Yamato-794046 chondrite and its inclusion, *Proc. NIPR Symp.*, *7*, 178–185.

Gaffey, M. J., and S. L. Gilbert (1998), Asteroid 6 Hebe: The probable parent body of the H-type ordinary chondrites and the IIE iron meteorites, *Meteorit. Planet. Sci.*, *33*, 1281–1295, doi:10.1111/j.1945-5100.1998.tb01312.x.

Gault, D. E., and J. A. Wedekind (1969), The destruction of tektites by meteoroid impact, *J. Geophys. Res.*, *74*, 6780–6794, doi:10.1029/JB074i027p06780.

Göpel, C., G. Manhès, and C. J. Allègre (1994), U-Pb systematics of phosphates from equilibrated ordinary chondrites, *Earth Planet. Sci. Lett.*, *121*, 153–171, doi:10.1016/0012-821X(94)90038-8.

Grady, M. M. (2000), *Catalogue of Meteorites*, 696 pp., Cambridge Univ. Press, Cambridge, U. K.

Graf, T., and K. Marti (1995), Collisional history of H chondrites, *J. Geophys. Res.*, *100*, 21,247–21,263, doi:10.1029/95JE01903.

Grier, J. A., D. A. Kring, T. D. Swindle, A. S. Rivkin, B. A. Cohen, and D. T. Britt (2004), Analyses of the chondritic meteorite Orvinio (H6), Insight into the origins and evolution of shocked H chondrite material, *Meteorit. Planet. Sci.*, *39*, 1475–1493, doi:10.1111/j.1945-5100.2004.tb00123.x.

Grieve, R. A. F. (1978), The melt rocks at Brent Crater, Ontario, Canada, *Proc. Lunar Planet. Sci. Conf.*, *9th*, 2579–2608.

Grieve, R. A. F. (1987), Terrestrial impact structures, *Annu. Rev. Earth Planet. Sci.*, *15*, 245–270, doi:10.1146/annurev.ea.15.050187.001333.

Grieve, R. A. F., M. R. Dence, and P. B. Robertson (1977), Cratering processes: As interpreted from the occurrence of impact melts, in *Impact and Explosion Cratering: Planetary and Terrestrial Implications*, edited by D. J. Roddy et al., pp. 791–814, Pergamon, New York.

Grimm, R. E. (1985), Penecontemporaneous metamorphism, fragmentation, and reassembly of ordinary chondrite parent bodies, *J. Geophys. Res.*, *90*, 2022–2028, doi:10.1029/JB090iB02p02022.

Grimm, R. E., W. F. Bottke, D. D. Durda, B. Enke, E. R. D. Scott, E. Asphaug, and D. Richardson (2005), Joint thermal and collisional modeling of the H chondrite parent body, *Lunar Planet. Sci.*, *XXXVI*, Abstract 1798.

Hevey, P. J., and I. S. Sanders (2006), A model for planetesimal meltdown by ^{26}Al and its implications for meteorite parent bodies, *Meteorit. Planet. Sci.*, *41*, 95–106, doi:10.1111/j.1945-5100.2006.tb00195.x.

Holsapple, K., I. Giblin, K. Housen, A. Nakamura, and E. Ryan (2002), Asteroid impacts: Laboratory experiments and scaling laws, in *Asteroids III*, edited by W. F. J. Bottke Jr. et al., pp. 443–462, Univ. of Ariz. Press, Tucson.

Hopfe, W. D., and J. I. Goldstein (2001), The metallographic cooling rate method revised Application to iron meteorites and mesosiderites, *Meteorit. Planet. Sci.*, *36*, 135–154, doi:10.1111/j.1945-5100.2001.tb01815.x.

Housen, K. (2009), Cumulative damage in strength-dominated collisions of rocky asteroids: Rubble piles and brick piles, *Planet. Space Sci.*, *57*, 142–153, doi:10.1016/j.pss.2008.07.006.

Keil, K., R. V. Fodor, P. M. Starzyk, R. A. Schmitt, D. D. Bogard, and L. Husain (1980), A 3.6-b.y.-old impact-melt rock fragment in the Plainview chondrite: Implications for the age of the H-group chondrite parent body regolith formation, *Earth Planet. Sci. Lett.*, *51*, 235–247, doi:10.1016/0012-821X(80)90207-1.

Keil, K., H. Haack, and E. R. D. Scott (1994), Catastrophic fragmentation of asteroids: Evidence from meteorites, *Planet. Space Sci.*, *42*, 1109–1122, doi:10.1016/0032-0633(94)90011-6.

Keil, K., D. Stöffler, S. G. Love, and E. R. D. Scott (1997), Constraints on the role of impact heating and melting in asteroids, *Meteorit. Planet. Sci.*, *32*, 349–363, doi:10.1111/j.1945-5100.1997.tb01278.x.

Kleine, T., M. Touboul, J. A. Van Orman, B. Bourdon, C. Maden, K. Mezger, and A. N. Halliday (2008), Hf–W thermochronometry: Closure temperature and constraints on the accretion and cooling history of the H chondrite parent body, *Earth Planet. Sci. Lett.*, *270*, 106–118, doi:10.1016/j.epsl.2008.03.013.

Kojima, H. (Ed.) (2001), Meteorite Newsletter 10(1), 60 pp., Natl. Inst. of Polar Res., Tokyo.

Kojima, H., and N. Imae (Eds.) (1998), Meteorites News 7(1), 95 pp., Natl. Inst. of Polar Res., Tokyo.

Kojima, H., and N. Imae (Eds.) (2000), Meteorite News 9(1), 58 pp., Natl. Inst. of Polar Res., Tokyo.

Kojima, H., and N. Imae (Eds.) (2002), Meteorite Newsletter 11(1), 49 pp., Natl. Inst. of Polar Res., Tokyo.

Kojima, H., and N. Imae (Eds.) (2003), Meteorite Newsletter 12(1), 52 pp., Natl. Inst. of Polar Res., Tokyo.

Kojima, H., and A. Yamaguchi (Eds.) (2005), Meteorite Newsletter 13(1), 24 pp., Natl. Inst. of Polar Res., Tokyo.

Kojima, H., and A. Yamaguchi (Eds.) (2007), Meteorite Newsletter 15, 15 pp., Antarct. Meteor. Res. Cent., Natl. Inst. of Polar Res., Tokyo.

Kojima, H., and A. Yamaguchi (Eds.) (2008), Meteorite Newsletter 16, 24 pp., Antarct. Meteor. Res. Cent., Natl. Inst. of Polar Res., Tokyo.

Kojima, H., and K. Yanai (Eds.) (1996), Meteorites News 6(1), 48 pp., Natl. Inst. of Polar Res., Tokyo.

Kojima, H., N. Imae, and A. Yamaguchi (Eds.) (2009), Meteorite Newsletter 18, 17 pp., Antarct. Meteor. Res. Cent., Natl. Inst. of Polar Res., Tokyo.

Korochantseva, E. V., A. I. Buikin, C. A. Lorenz, J. Hopp, W. H. Schwarz, and M. Trieloff (2008), ^{40}Ar-^{39}Ar dating of a melt inclusion from Dhofar 323(H5), An early impact event, Goldschmidt Conference, *Geochim. Cosmochim. Acta*, *72*, suppl., A491.

Kring, D. A., and B. A. Cohen (2002), Cataclysmic bombardment throughout the inner solar system 3.9–4.0 Ga, *J. Geophys. Res.*, *107*(E2), 5009, doi:10.1029/2001JE001529.

Kring, D. A., T. D. Swindle, D. T. Britt, and J. A. Grier (1996), Cat Mountain: A meteoritic sample of an impact-melted asteroid regolith, *J. Geophys. Res.*, *101*, 29,353–29,371, doi:10.1029/96JE03139.

Kring, D. A., D. H. Hill, J. D. Gleason, D. T. Britt, G. J. Consolmagno, M. Farmer, S. Wilson, and R. Haag (1999), Portales Valley: A meteoritic sample of the brecciated and metal-veined floor of an impact crater on an H chondrite asteroid, *Meteorit. Planet. Sci.*, *34*, 663–669, doi:10.1111/j.1945-5100.1999.tb01372.x.

Kring, D. A., B. A. Cohen, T. D. Swindle, and D. H. Hill (2000), Regolith breccia (Ourique) with impact melt clasts and other debris from an H chondrite parent body, *Lunar Planet. Sci.*, Abstract 1688.

Kunz, J., M. Falter, and E. K. Jessberger (1997), Shocked meteorites: ^{40}Ar-^{39}Ar evidence for multiple impacts, *Meteorit. Planet. Sci.*, *32*, 647–670, doi:10.1111/j.1945-5100.1997.tb01550.x.

Leitch, C. A., and L. Grossman (1977), Lithic clasts in the Supuhee chondrite, *Meteoritics*, *12*, 125–139.

Lipschutz, M. E., and L. Schultz (2007), Meteorites, in *Encyclopedia of the Solar System*, edited by L.-A. McFadden et al., pp. 251–282, Academic, San Diego, Calif. doi:10.1016/B978-012088589-3/50017-7.

Mason, B. (1965), The chemical composition of olivine-bronzite and olivine-hypersthene chondrites, *Am. Mus. Novit.*, *2223*, 1–38.

McSween, H. Y., Jr., M. E. Bennett III, and E. Jarosewich (1991), The mineralogy of ordinary chondrites and implications for asteroid spectrophotometry, *Icarus*, *90*, 107–116, doi:10.1016/0019-1035(91)90072-2.

McSween, H., Jr., A. Ghosh, R. E. Grimm, L. Wilson, and E. D. Young (2002), Thermal evolution models of asteroids, in *Asteroids III*, edited by W. F. Bottke Jr. et al., pp. 559–571, Univ. of Ariz. Press, Tucson.

Michel, P., W. Benz, and D. C. Richardson (2003), Disruption of fragmented parent bodies as the origin of asteroid families, *Nature*, *421*, 608–611, doi:10.1038/nature01364.

Ming, C., X. Xiande, and A. El Goresy (1995), Nonequilibrium solidification and microstructures of metal phases in the shock-induced melt of the Yanzhuang (H6) chondrite, *Meteoritics*, *30*, 28–32.

Nesvorný, D., W. F. Bottke, D. Vokrouhlický, A. Morbidelli, and R. Jedicke (2005), Asteroid families, in *Asteroids, Comets, Meteors: Proceedings of the 229th Symposium of the International Astronomical Union Held in Buúzios, Rio de Janeiro, Brasil, August 7–12, 2005*, edited by D. Lazzaro et al., pp. 289–299, Cambridge Univ. Press, Cambridge, U. K.

Niihara, T., N. Imae, and H. Kojima (2007), Petrography of Yamato-791088, a heavily shocked H chondrite, paper presented at 31st Symposium on Antarctic Meteorites, pp. 73–74, Natl. Inst. of Polar Res., Tokyo.

Onorato, P. I. K., D. R. Uhlmann, and C. H. Simonds (1978), The thermal history of the Manicouagan impact melt sheet, *J. Geophys. Res.*, *83*, 2789–2798, doi:10.1029/JB083iB06p02789.

Rubin, A. E., and W. F. Bottke (2009), On the origin of shocked and unshocked CM clasts in H chondrite regolith breccias, *Meteorit. Planet. Sci.*, *44*, 701–724, doi:10.1111/j.1945-5100.2009.tb00764.x.

Rubin, A. E., and R. H. Jones (2003), Spade: An H chondrite impact-melt breccia that experienced post-shock annealing, *Meteorit. Planet. Sci.*, *38*, 1507–1520, doi:10.1111/j.1945-5100.2003.tb00254.x.

Russell, S. S., M. Zolensky, K. Righter, L. Folco, R. Jones, H. C. J. Connolly, M. M. Grady, and J. N. Grossman (2005), The Meteoritical Bulletin, No. 89, 2005 September, *Meteorit. Planet. Sci.*, *40*, suppl., A201–A263, doi:10.1111/j.1945-5100.2005.tb00425.x.

Ruzicka, A., G. A. Snyder, and L. A. Taylor (1998), Mega-chondrules and large, igneous-textured clasts in Julesberg (L3) and other ordinary chondrites: Vapor-fractionation, shock-melting, and chondrule formation, *Geochim. Cosmochim. Acta*, *62*, 1419–1442, doi:10.1016/S0016-7037(98)00029-5.

Ruzicka, A., M. Killgore, D. W. Mittlefehldt, and M. D. Fries (2005), Portales Valley: Petrology of a metallic-melt meteorite breccia, *Meteorit. Planet. Sci.*, *40*, 261–295, doi:10.1111/j.1945-5100.2005.tb00380.x.

Sack, R. O., M. S. Ghiorso, M.-S. Wang, and M. E. Lipschutz (1994), Igneous inclusions from ordinary chondrites: High temperature cumulates and a shock melt, *J. Geophys. Res.*, *99*, 26,029–26,044, doi:10.1029/94JE02709.

Sahijpal, S., P. Soni, and G. Gupta (2007), Numerical simulations of the differentiation of accreting planetesimals with ^{26}Al and ^{60}Fe as the heat sources, *Meteorit. Planet. Sci.*, *42*, 1529–1548, doi:10.1111/j.1945-5100.2007.tb00589.x.

Schwarz, W. H., M. Trieloff, E. V. Korochantseva, and A. I. Buikin (2006), New data on the cooling history of the H chondrite parent body, *Meteorit. Planet. Sci.*, *41*, A161.

Scott, E. R. D. (1982), Origin of rapidly solidified metal-troilite grains in chondrites and iron meteorites, *Geochim. Cosmochim. Acta*, *46*, 813–823, doi:10.1016/0016-7037(82)90032-1.

Sepp, B., A. Bischoff, and D. Bosbach (2001), Low-temperature phase decomposition in iron-nickel metal of the Portales Valley meteorite, *Meteorit. Planet. Sci.*, *36*, 587–595, doi:10.1111/j.1945-5100.2001.tb01902.x.

Smith, B. A., and J. I. Goldstein (1977), The metallic microstructures and thermal histories of severely reheated chondrites, *Geochim. Cosmochim. Acta*, *41*, 1061–1072, doi:10.1016/0016-7037(77)90100-4.

Stöffler, D., and R. A. F. Grieve (2007), Impactites, in *Metamorphic Rocks: A Classification and Glossary of Terms, Recommendations of the International Union of Geological Sciences Subcommission on the Systematics of Metamorphic Rocks*, edited by D. Fettes and J. Desmons, pp. 82–242, Cambridge Univ. Press, Cambridge, U. K.

Stöffler, D., K. Keil, and E. R. D. Scott (1991), Shock metamorphism of ordinary chondrites, *Geochim. Cosmochim. Acta*, *55*, 3845–3867, doi:10.1016/0016-7037(91)90078-J.

Sullivan, R., et al. (1996), Geology of 243 Ida, *Icarus*, *120*, 119–139, doi:10.1006/icar.1996.0041.

Swindle, T. D., C. E. Isachsen, J. R. Weirich, and D. A. Kring (2009), ^{40}Ar-^{39}Ar ages of H chondrite impact melt breccias, *Meteorit. Planet. Sci.*, *44*, 747–762, doi:10.1111/j.1945-5100.2009.tb00766.x.

Tagle, R., T. Öhman, R. T. Schmitt, J. Erzinger, and P. Claeys (2007), Traces of an H chondrite in the impact-melt rocks from the Lappajärvi impact structure, Finland, *Meteorit. Planet. Sci.*, *42*, 1841–1854, doi:10.1111/j.1945-5100.2007.tb00542.x.

Taylor, G. J., and D. Heymann (1971), Postshock thermal histories of reheated chondrites, *J. Geophys. Res.*, *76*, 1879–1893, doi:10.1029/JB076i008p01879.

Taylor, G. J., K. Keil, J. L. Berkley, and D. L. Lange (1979), The Shaw meteorite: History of a chondrite consisting of impact-melted and metamorphic lithologies, *Geochim. Cosmochim. Acta*, *43*, 323–337, doi:10.1016/0016-7037(79)90198-4.

Taylor, G. J., P. Maggiore, E. R. D. Scott, A. E. Rubin, and K. Keil (1987), Original structure, and fragmentation and reassembly histories of asteroids: Evidence from meteorites, *Icarus*, *69*, 1–13, doi:10.1016/0019-1035(87)90002-9.

Tera, F., D. A. Papanastassiou, and G. J. Wasserburg (1974), Isotopic evidence for a terminal lunar cataclysm, *Earth Planet. Sci. Lett.*, *22*, 1–21, doi:10.1016/0012-821X(74)90059-4.

Thompson, L. M., and J. G. Spray (1994), Pseudotachylite rock distribution and genesis within the Sudbury impact structure, in *Large Meteorite Impacts and Planetary Evolution*, edited by B. O. Dressler et al., pp. 275–287, Geol. Soc. of Am., Boulder, Colo.

Trieloff, M., E. K. Jessberger, I. Herrwerth, J. Hopp, I. Fieni, M. Ghelis, M. Bourot-Denise, and P. Pellas (2003), Structure and thermal history of the H chondrite parent asteroid revealed by thermometry, *Nature*, *422*, 502–506, doi:10.1038/nature01499.

Turner, G., P. H. Cadogan, and C. Y. Yonge (1973), Argon selenochronology, *Proc. Lunar Sci. Conf.*, *4th*, 1889–1914.

Turner, G., M. C. Enright, and P. H. Cadogan (1978), The early history of chondrite parent bodies inferred from ^{40}Ar-^{39}Ar ages, *Proc. Lunar Planet. Sci. Conf.*, *9th*, 978–1025.

van der Bogert, C. H., P. H. Schultz, and J. G. Spray (2003), Impact-induced frictional melting in ordinary chondrites: A mechanism for deformation, darkening, and vein formation, *Meteorit. Planet. Sci.*, *38*, 1521–1531, doi:10.1111/j.1945-5100.2003.tb00255.x.

Van Schmus, W. R., and J. A. Wood (1967), A chemical-petrologic classification for the chondritic meteorites, *Geochim. Cosmochim. Acta*, *31*, 747–765, doi:10.1016/S0016-7037(67)80030-9.

Weidenschilling, S. J., and J. N. Cuzzi (2006), Accretion dynamics and timescales: Relation to chondrites, in *Meteorites in the Earth Solar System II*, edited by D. Lauretta and H. McSween, pp. 473–485, Univ. of Ariz. Press, Tucson.

Weisberg, M. K., C. Smith, G. Benedix, L. Folco, K. Righter, J. Zipfel, A. Yamaguchi, and H. C. Aoudjehane (2008), The Meteoritical Bulletin, No. 94, September 2008, *Meteorit. Planet. Sci.*, *43*, 1551–1584, doi:10.1111/j.1945-5100.2008.tb01027.x.

Winter, J. D. (2001), *An Introduction to Igneous and Metamorphic Petrology*, 697 pp., Prentice-Hall, Upper Saddle River, N. J.

Wittmann, A., J. A. Weirich, T. D. Swindle, D. Rumble III, and D. A. Kring (2009), Petrography of MIL05029, the first accretional impact melt from the L chondrite parent body, *Lunar Planet. Sci.*, *XL*, Abstract 1426.

Yang, C. W., D. B. Williams, and J. I. Goldstein (1996), A revision of the Fe-Ni phase diagram at low temperatures (<400°C), *J. Phase Equilibria*, *17*, 522–531, doi:10.1007/BF02665999.

L. C. Cheek, Department of Geological Sciences, Brown University, Providence, RI 02912, USA. (Leah_Cheek@brown.edu)

E. A. Frank, Department of Earth and Environmental Sciences, Rensselaer Polytechnic Institute, Troy, NY 12180, USA. (elizabeth.frank@alum.rpi.edu)

D. A. Kring and A. Wittmann, Lunar and Planetary Institute, 3600 Bay Area Blvd., Houston, TX 77058, USA. (wittmann@lpi.usra.edu; kring@lpi.usra.edu)

T. D. Swindle, Lunar and Planetary Laboratory, University of Arizona, Tucson, AZ 85721, USA. (tswindle@U.Arizona.edu)